

**Palacký University Olomouc, Faculty of Science,
Department of Geoinformatics**

**Paris Lodron University Salzburg, Faculty of Natural Sciences,
Department of Geoinformatics**

MAPPING AND VISUALISING LAVA FLOWS OF THE FAGRADALSFJALL VOLCANO IN ICELAND

Diploma thesis

Author

Sofia Margarita DELGADO BALAGUERA

Supervisor (Palacký University Olomouc)
RNDr. Jan BRUS, Ph.D.

Co-supervisor (Paris Lodron University Salzburg)
Dr. Daniel Hölbling, Ph.D.

**Erasmus Mundus Joint Master Degree Programme
Copernicus Master in Digital Earth
Specialization Track Geovisualization & Geocommunication
Olomouc, Czech Republic, 2023**



Palacký University
Olomouc



ANOTATION

The Fagradalsfjall volcanic system in Iceland erupted in March 2021 marking the end of a long dormancy period in the Reykjanes Peninsula. Mapping, analysing, and visualising volcanic hazards such as lava flows play an essential role in disaster risk management and increases general awareness of their possible danger. This research elaborated a time-series analysis to delineate the extent of the lava flows generated during the 2021 Fagradalsfjall eruption using Synthetic Aperture Radar and Object-based Image Analysis, validated and compared the delineation of the resulting lava flow outlines with existing reference data, and interactively visualised the lava flow field evolution. The calculated area of the lava flow path resulted in 4,3 km², ten percent less than the area reported for previous delineations. The validation of the results indicated high correlation and coincidence with the reference data and displayed accuracies above 80%. The results of the application of the OBIA method on Sentinel-1 backscatter data revealed certain potential for lava flow mapping as they showed agreement with existing reference data, however, the outcomes should be evaluated carefully since factors such as spatial resolution, Synthetic Aperture Radar (SAR) geometrical distortions, and the OBIA segmentation scheme can influence the classification. The web application provides an interactive framework to communicate the results of the research. Further studies could make use of the lava flow delineation as inputs for lava modelling or as ground data for future eruptions of the Fagradalsfjall volcano. Furthermore, the contribution can support local authorities to promptly respond to lava flow potential danger.

KEYWORDS

Fagradalsfjall eruption 2021, synthetic aperture radar, object-based image analysis, Sentinel-1, web application

Number of pages 46

Number of appendixes 2

DECLARATION

This thesis has been composed by *Sofia Margarita Delgado Balaguera* for the Erasmus Mundus Joint Master's Degree Program in Copernicus Master in Digital Earth for the academic years 2021/2022 and 2022/2023 at the Department of Geoinformatics, Faculty of Natural Sciences, Paris Lodron University Salzburg, and Department of Geoinformatics, Faculty of Science, Palacký University Olomouc.

Hereby, I declare that this piece of work is entirely my own, the references cited have been acknowledged and the thesis has not been previously submitted to the fulfilment of the higher degree.

12.05.2021, Olomouc

Sofia Margarita Delgado Balaguera

ACKNOWLEDGEMENT

Thanks to my supervisors for their suggestions and comments during the elaboration of the work. I thank the Planet's Education and Research Program that sponsored me with access to their imagery for research purposes and the Trimble Innovation Programme that together with the Department of Geoinformatics – Z_GIS from the University of Salzburg provided me with the eCognition license.

Palacký University Olomouc
Faculty of Science
Academic year: 2022/2023

ASSIGNMENT OF DIPLOMA THESIS

(project, art work, art performance)

Name and surname: Sofia Margarita DELGADO BALAGUERA
Personal number: R210701
Study programme: N0532A330010 Geoinformatics and Cartography
Work topic: Mapping and visualizing lava flows of the Fagradalsfjall volcano in Iceland
Assigning department: Department of Geoinformatics

Theses guidelines

The main aim of the thesis is elaborate a time-series analysis to delineate the extent of the lava flows generated during the volcanic eruption of Fagradalsfjall volcano using Earth Observation data. The student will validate and compare her delineation based on radar data with optical imagery and existing delineations. The second aim is to interactively visualize the time-series analysis of lava flow field evolution and create animations.

The student will attach all the collected datasets to the thesis in digital form. The student will create a website about the thesis following the rules available on the department's website and a poster about the diploma thesis in A2 format. The student will submit the entire text (text, attachments, poster, outputs, input and output data) in digital form on a storage medium and the text of the thesis in two bound copies to the department's secretary.

Extent of work report: max 50 pages
Extent of graphics content: as needed
Form processing of diploma thesis: printed
Language of elaboration: English

Recommended resources:

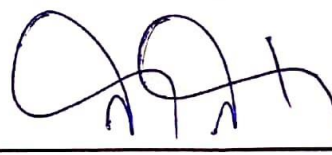
- Corradino, C., Bilotta, G., Cappello, A., Fortuna, L., & Del Negro, C. (2021). Combining radar and optical satellite imagery with machine learning to map lava flows at Mount Etna and Fogo Island. *Energies*, 14(1), 197.
- Hölbling, D., Auffermann, M., & Dabiri, Z. (2019). Object-based Image Analysis for Lava Flow Morphology Classification using Optical and SAR Satellite Imagery. In *27th IUGG General Assembly 2019*.
- Palomà, R., Monserrat, O., Crippa, B., Crosetto, M., Bru, G., Ezquerro, P., & Bejar-Pizarro, M. (2022, July). Generation of a Digital Elevation Model Using Capella High-Resolution SAR Data: First Results Over La Palma Island. In *IGARSS 2022-2022 IEEE International Geoscience and Remote Sensing Symposium* (pp. 3472-3475). IEEE.
- Sbrana, A., Cioni, R., Marianelli, P., Sulpizio, R., Andronico, D., & Pasquini, G. (2020). Volcanic evolution of the Somma-Vesuvius complex (Italy). *Journal of Maps*, 16(2), 137-147.
- Poland, M. P. (2022). Synthetic aperture radar volcanic flow maps (SAR VFMs): A simple method for rapid identification and mapping of volcanic mass flows. *Bulletin of Volcanology*, 84(3), 32.
- Watson, A., Kennedy, B. M., Jolley, A., Davidson, J., & Brogt, E. (2022). Design, implementation, and insights from a volcanology Virtual Field Trip to Iceland. *Volcanica*, 5(2), 451-467.

Supervisors of diploma thesis: RNDr. Jan Brus, Ph.D.
Department of Geoinformatics

Date of assignment of diploma thesis: December 5, 2022
Submission deadline of diploma thesis: May 5, 2023

LS.

doc. RNDr. Martin Kubala, Ph.D.
Dean



prof. RNDr. Vít Voženílek, CSc.
Head of Department

CONTENT

LIST OF ABBREVIATIONS	7
INTRODUCTION	8
1 OBJECTIVES.....	10
2 STATE OF ART.....	11
3 METHODOLOGY	16
3.1 Study Area	16
3.2 Methods	17
3.3 Data	18
3.4 Software	19
3.5 Processing procedure	20
4 LAVA FLOW MAPPING	21
4.1 Data collection and pre-processing.....	21
4.2 Lava flow delineation	26
4.3 Validation.....	34
5 LAVA FLOWS VISUALISATION	35
5.1 Pre-processing.....	35
5.2 Visualisation	36
6 RESULTS	39
6.1 Lava flow mapping results.....	39
6.2 Visualisation results	41
7 DISCUSSION	43
8 CONCLUSION	46
REFERENCES AND INFORMATION SOURCES	
ATTACHMENTS	

LIST OF ABBREVIATIONS

Abbreviation	Meaning
EO	Earth Observation
SAR	Synthetic Aperture Radar
OBIA	Object-based Image Analysis
RP	Reykjanes Peninsula
MW	Moment Magnitude
InSAR	Interferometric Synthetic Aperture Radar
LOS	Line of Sight
GNSS	Global Navigation Satellite System
DEM	Digital Elevation Model
ESA	European Space Agency
SL	Subtraction layer
HTML	HyperText Markup Language
JS	JavaScript
CSS	Cascading Style Sheet
MASL	Meters Above the Sea Level

INTRODUCTION

Understanding and identifying volcanic hazards plays an essential role in disaster risk management. Volcanic eruptions and their associated processes can drastically impact human lives and cause socioeconomic disruption. Space-based technologies provide a comprehensive and methodical frame of reference for a better understanding of volcanic processes leading to disasters. Assessments of volcanic parameters and related risks are increasingly incorporating remote sensing data and techniques. This is because of the capability of Earth observation (EO) data to capture thermal anomalies, ground deformation, and ash dispersal within different portions of the electromagnetic spectrum (Cigna et al., 2020). Moreover, to monitor the development and progress of volcanic processes, it is necessary to utilise high-temporal resolution data that regularly document and track such events. Thus, the integration of EO data with volcanic deposits mapping and analysis allows for the improvement of risk assessment models, near-real-time monitoring, and decision-making processes.

Iceland is frequently subject to volcanic activity due to its location in a divergent plate boundary. The most common volcanic hazards in Iceland are lava flows, pyroclastic density currents, tephra fallout, lightning, and pollution (Gudmundsson et al., 2008). Lava flows are usually localised and slow-motion volcanic events that can be hazardous because of their extreme temperatures and capacity to surround, bury, or create structural failures (Harris, 2015). Large effusive eruptions are frequently difficult to understand on the ground, especially when they are confined to remote or hardly accessible areas, representing a limitation for field data collection and frequent aerial surveying. Compared to field measurements, lava flow mapping using free satellite imagery is less time-consuming, cost-effective, and does not impose danger to human lives.

Although reliable lava flow mapping is also possible by the use of multispectral images, cloud cover frequently prevents their use. Besides, lava flow boundaries can be hard to distinguish with optical imagery when lava flow overlapping occurs (Smets et al., 2010). SAR data have been extensively used for volcanic monitoring, deformation, and lava flow mapping of different volcanic eruptions in Iceland (Dierking & Haack, 1998; Dirscherl & Rossi, 2018; Dumont et al., 2018). Due to SAR weather independence and day-and-night capabilities, this sensing system can provide data on a continuous basis, making it extremely useful for monitoring and tracking lava flow progress (Pinel et al., 2014). Moreover, Object-based image analysis (OBIA) has the potential for analysing the evolution of dynamic processes on Earth and has been widely used in geomorphological mapping. The main advantage of OBIA is that it uses additional dimensions of information about geographic entities, such as spectral, spatial, or textural properties compared to pixel-based approaches (Blaschke, 2005). However, lava flow mapping integrating OBIA and SAR backscatter information is scarce and only a few studies have been conducted (Aufaristama et al., 2017; Hölbling et al., 2019). Thus, further research in this direction is needed.

The aim of this study is to determine the evolution of the lava flow extent for the 2021 Fagradalsfjall eruption in Iceland using OBIA and Sentinel-1 data, to visualise the freely available data and the obtained lava outlines in an interactive way, and to evaluate the potential of freely available SAR data for semi-automated lava flow mapping.

1 OBJECTIVES

This diploma thesis aims to determine the evolution of the lava flow extent for the 2021 Fagradalsfjall eruption in Iceland using OBIA and Sentinel-1 data, to evaluate the potential of freely available SAR data for semi-automated lava flow mapping, and to visualise the lava flow fields interactively. The specific goals of the study are:

- 1) Elaborate a time-series analysis to delineate the extent of the lava flows generated during the volcanic eruption (~March to September 2021) using Sentinel-1 data and OBIA.
- 2) Validate and compare the resulting delineation with existing delineations of the lava flows (Pedersen et al., 2022) to evaluate the potential of SAR data for lava flow mapping.
- 3) Visualize the lava field outlines through the elaboration of a public 3D web map application as a user-friendly and communicative interface.

2 STATE OF ART

This chapter revises past and current investigations on the use of SAR and OBIA for lava flow and geomorphological mapping, which provide the most fundamental background for the development of the research aim. In this study, we explore the applicability of Sentinel-1 (C-band) SAR backscatter information together with OBIA to map the lava flows of the 2021 Fagradalsfjall eruption.

The 2021 eruption at Fagradalsfjall

The Fagradalsfjall volcano is located in the Reykjanes Peninsula (RP), Iceland. The RP allocates the Reykjanes Ridge and functions as a highly oblique divergent plate boundary pulling the North American and the Eurasian tectonic plates apart (Höskuldsson et al., 2007; Sigmundsson et al., 2022). The volcanic systems in the RP consist of networks of NE-SW trending fissure vents en-echelon acting as effusive basaltic lava fountains that expose geothermal areas and plume-ridge interaction (Clifton & Kattenhorn, 2006; Höskuldsson et al., 2007; Sæmundsson et al., 2020); however, the Fagradalsfjall system varies from other volcanic systems in the Peninsula as it does not exhibit geothermal fields or well-defined NE-SW trending swarms, and instead, it shows N-S trending faults that served as lava fountains (Global Volcanism Program, 2021; Sæmundsson et al., 2020). The vulcanism in the Peninsula for the past ~3000 years has shown eruptive episodes within a range of hundreds of years followed by dormancy periods of 800 to 1000 years (Sæmundsson et al., 2020). This eruption started on 19 March 2021 after a quiescence period of 6000 years in the Fagradalsfjall volcanic system and 781 years in the RP, and lasted for a period of 6 months, ending on 19 September 2021. Pre-eruptive seismicity and deformation along with inflation episodes preceded the volcanic activity, being the most representative an earthquake of magnitude MW 5.7 on 24 February 2021 (Lamb et al., 2022; Sigmundsson et al., 2022). Figure 1, elaborated by the Icelandic Meteorological Office, shows a Sentinel-1 image interferogram from 19 to 25 February 2021. The MW 5.7 earthquake position (24 February 2021) is given by the red star and the black arrows in the bottom-right corner represent the heading and looking direction of the satellite. The earthquake activity in the RP and the movement of the faulting systems along the plate boundary expose ground deformation in the area.

Four to five eruptive phases have been described for the Fagradalsfjall 2021 volcanic eruption by different authors considering temporal variations in lava outpouring, repose periods, heights reached by the lava, and changes in the lava time-average discharge rate. The following phases of the eruption have been documented by Pedersen et al. (2022) and Barsotti et al. (2023): The first phase of the eruption initiated with the opening of a 180 meters length fissure that rapidly became two different vents with fountaining activity filling the Geldingadallir valley. The second phase started on 05 April 2021 with the aperture of five additional vents and the active vent migration, extending the eruption to the northeast. The activity included bubble-bursting and outpouring of lava in variable amounts alternated between vents. The third phase began on 27 April 2021 and was characterized by an increase in the lava time-average discharge rate with lava fountains along with different intensities and periodicity from a single vent, which remained active for the rest of the eruption. Intermittent volcanic activity from 28 June 2021 marked the beginning of the fourth phase exposing non-continuous fountaining and episodes of strong lava emplacement alternated with repose intervals. Phase 5 was established on 02

September 2021, starting with a week-long pause in the volcanic activity followed by a week-long lava outpouring episode. By the end of the eruption on 18 September 2021, the estimated area covered by the lava flow was 4.8 km², the average lava discharge rate for most of the eruption was 9.5 m³/s, and the mean lava thickness was estimated above 30 meters according to Pedersen et al. (2022).

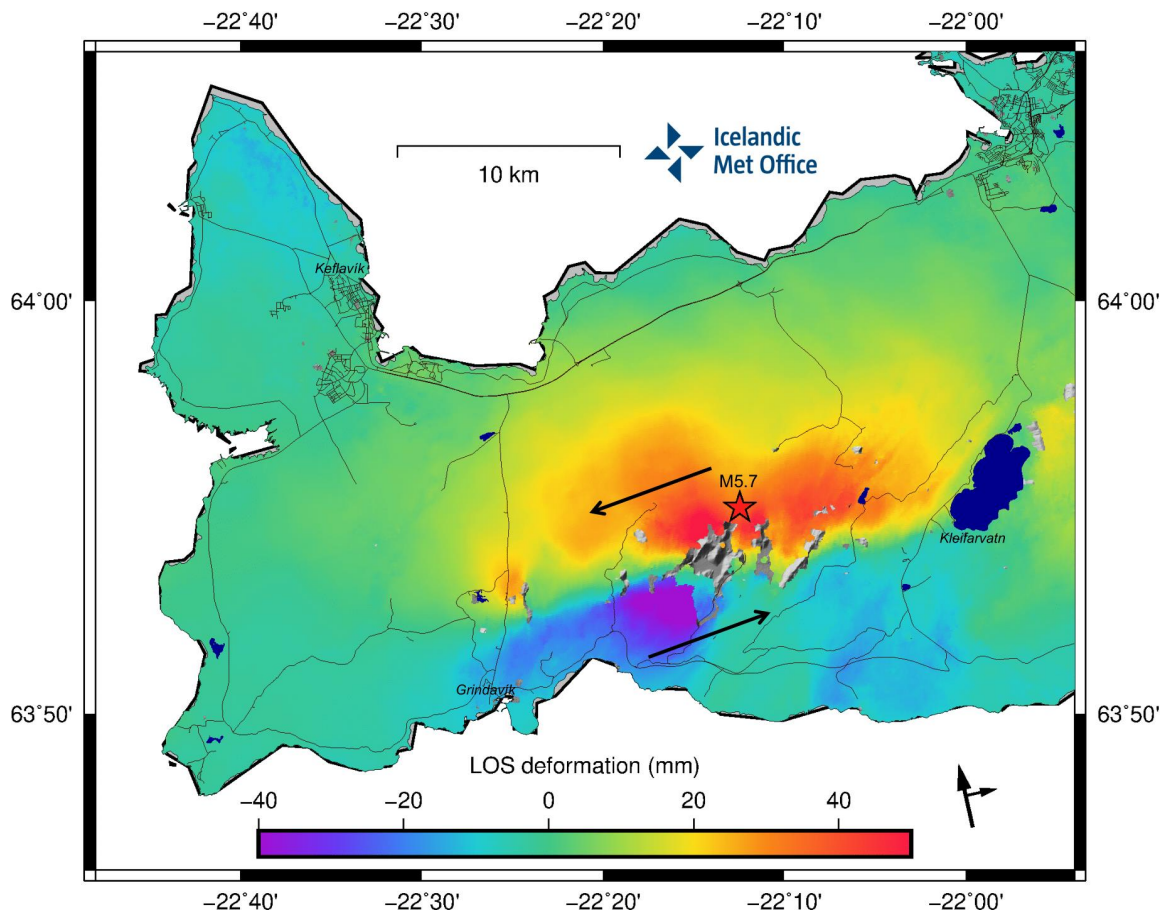


Figure 1: InSAR interferogram showing the Line of Sight (LOS) deformation in the area (source: <https://www.vedur.is/um-vi/frettir/ekkert-hraunflaedi-i-thrja-manudi-vid-fagradalsfjall>).

SAR data applications in lava flow monitoring

SAR is an active remote sensing technology that operates in the microwave region of the electromagnetic spectrum. SAR weather independence and day-and-night capabilities allow continuous data collection, making this sensing system suitable for imaging large areas and for monitoring and tracking the course of lava flows (Pinel et al., 2014). The use of SAR data has been extensively applied in volcanic monitoring, surface deformation measuring, and lava flow mapping of different volcanic eruptions.

Interferometric SAR (InSAR) refers to an imaging technique that exploits the phase information of the coherent radar signal for measuring electrical and geometrical properties of the surface and its changes over time (Rosen et al., 2000). The extended usage of InSAR in volcanology is due to the capability of this technique to image the

spatial and temporal extent of volcanic surface motion, offering insights into the eruptive behavior and stability of the volcanic structure (Rosen et al., 2000). Because volcanic structures such as dikes and sills exhibit individual deformation patterns when the magma intrudes, the deformation measurements extracted from InSAR can be used to model the magma chamber in depth, size, and shape (Zhou et al., 2009). Therefore, InSAR has been applied in lava flow monitoring to measure surface deformation at several volcanoes around the world (e.g., Aditiya et al., 2018; Kyriou & Nikolakopoulos, 2022; Richter & Froger, 2020; Romero et al., 2002; Samsonov & d'Oreye, 2012). Additionally, InSAR phase delays can be used to create multi-temporal DEMs to estimate lava flow changes in height and volume and extrusion rates between different acquisitions (e.g., Albino et al., 2015; Dumont et al., 2018; Ebmeier et al., 2012; Kubanek et al., 2015).

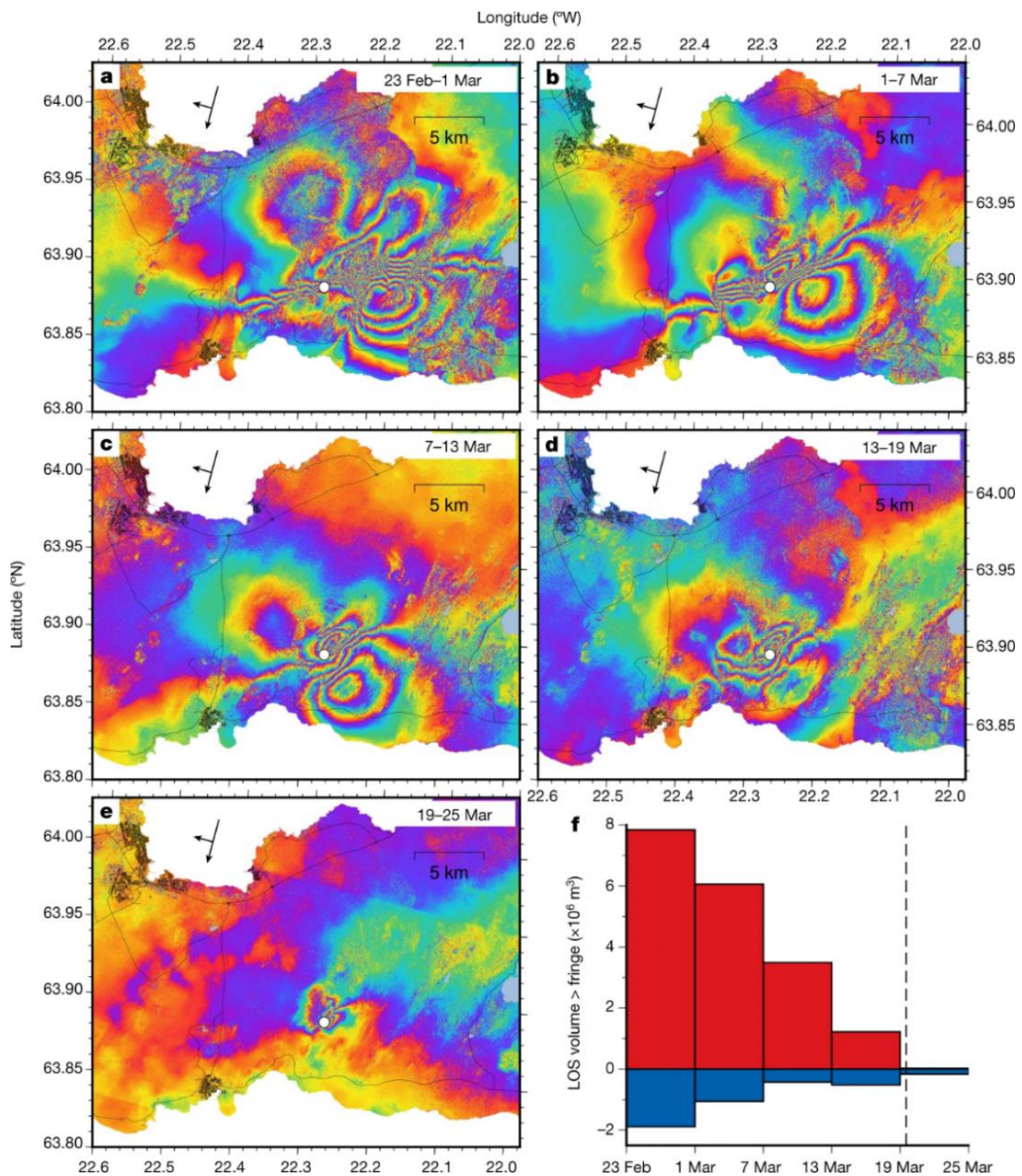


Figure 2: Spatial and temporal evolution of deformation before the 2021 Fagradalsfjall eruption. (Sigurdsson et al., 2022).

Sigmundsson et al. (2022) modelled the surface deformation in the Fagradalsfjall area before the start of the 2021 eruption using InSAR analysis and Global Navigation Satellite System (GNSS) geodesy. Interferograms were created from Sentinel-1 data to observe the displacement along the LOS from 24 February 2021 when the MW 5.7 earthquake occurred until 19 March 2021 when the eruption started. The model showed that the deformation rate decreased over time along with systematic tectonic stress release and reached its lowest point at the eruption onset. Figure 2 shows the LOS change in Sentinel-1 InSAR interferograms obtained by Sigmundsson et al. (2022). The position of the eruption site is given by the white dot and the black arrows represent the heading and looking direction of the satellite. On the other hand, InSAR analysis using daily ICEYE X-band satellite imagery was carried out by Drouin et al., 2022 for measuring ground deformation during the 2021 Fagradalsfjall eruption. The measurements allowed the observation of the opening of eruptive fissures throughout the eruption and provided insights for modeling the subsurface magma path.

Lava flow mapping with OBIA

OBIA has been widely used in geomorphological mapping as it has the potential to analyse the evolution of dynamic processes on Earth. Change detection integrated with object-based image analysis (OBIA) has the potential for analysing the evolution of dynamic processes on Earth (Chen et al., 2012). The traditional pixel-based change detection method uses single pixels as the main unit for analysis. Conversely, the OBIA approach groups pixels as image objects that represent meaningful features by using additional dimensions of information about the geographic entities such as spectral, spatial, geographical, and textural information of the geographic entities (Blaschke, 2005). Furthermore, traditional mapping methods such as manual delineation of lava flows can be costly and time-consuming when compared to OBIA, making it a very efficient and appropriate technique for the identification and classification of volcanic deposits, including lava flows (Feizizadeh et al., 2021; Pedersen, 2016).

Different studies have demonstrated the suitability of OBIA for lava flow mapping and lava morphology classification (e.g., Aufaristama et al., 2017; Feizizadeh et al., 2021; Hölbling et al., 2019; Pedersen, 2016; Rösch & Plank, 2022). However, the methodology has been applied mostly to optical imagery or terrain model derivatives, indicating that the additional dimensions of SAR backscatter information together with OBIA have not been thoroughly exploited. For instance, Pedersen (2016) utilised an object-based mapping approach to semi-automatically classify glaciovolcanic landforms from the Reykjanes Peninsula in Iceland. The methodology tested OBIA on geomorphometric features such as slope and profile curvature that were extracted from a high-resolution digital elevation model of the area. The results of the classification were tested against a geological map using an error matrix and compared to the classified area for lava plains and hyaloclastite within the volcanic zone. The overall accuracy exceeded 90% evidencing a great performance of the procedure for glaciovolcanic landforms classification. Additionally, the author concluded that in comparison to OBIA classification schemes based on spectral features, the approach deals properly with complex volcanic edifices configurations, solves potential issues associated with vegetation cover, and allows a better integration with GIS environments which makes it more transferrable.

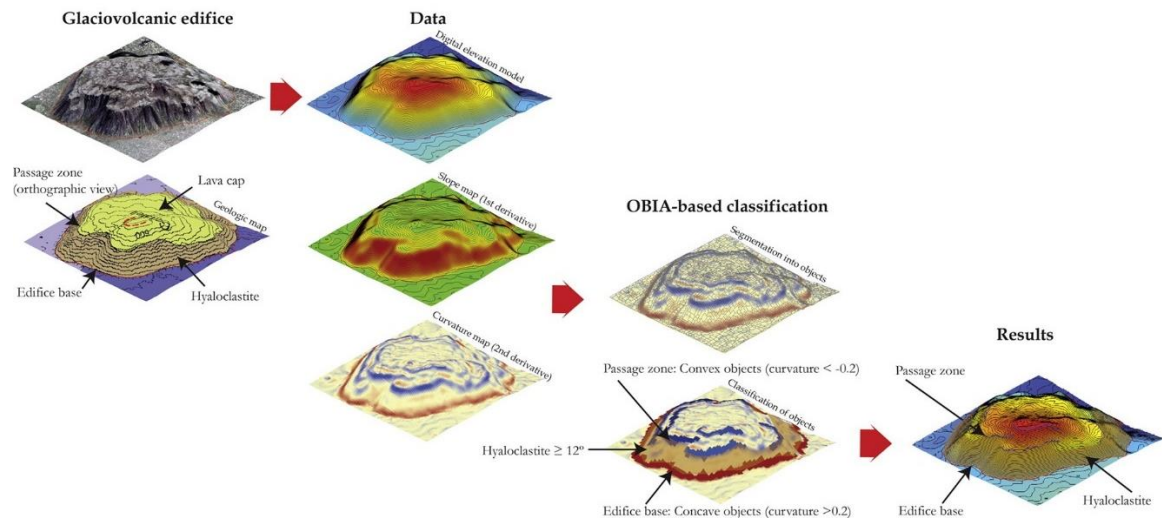


Figure 3: Workflow for glaciovolcanic landform and landform element classification (Pedersen, 2016)

Another study by Hölbling et al. (2019) classified the lava flow morphology of the Krafla volcano lava field in Iceland using OBIA and Sentinel-1 and 2 imageries. The methodology included a multiresolution segmentation and a supervised classification using the random forest machine learning algorithm. When compared to a reference dataset, the classification resulted in accuracies from 28% up to 90% depending on the type of lava, suggesting the high potential of automated classification on optical and SAR data for differentiating lava flow morphologies.

Feizizadeh et al. (2021) developed a semi-automated approach for delineating volcanic landforms in the Sahand Mountain in Iran using OBIA. The procedure comprised a multiresolution segmentation applied on Sentinel-2 data followed by a fuzzy-based nearest neighbour classification algorithm that utilised spectral, geometric, and textural information provided by the optical imagery, along with spatial information derived from a DEM such as altitude, slope, and flow accumulation. The overall accuracies for the lava flow classes resulted in more than 90% demonstrating the efficiency of the methodology for detecting and classifying volcanic landforms.

Web mapping applications in volcanic contexts

Over the past few decades, web mapping and the use of geospatial data on the web have increased (Veenendaal et al., 2017). Interactive web map applications in the context of natural sciences provide meaningful geographic information to users in an effective and engaging way. Through interactive and 3D visualization, immersion into the story and the presented data is facilitated (Thöny et al., 2018). Besides, storytelling in cartography and geography provides a method for documenting, communicating, and sharing spatial information, and improves map readability for a diverse group of users, including non-experts (Roth, 2021). Some authors have created interactive web map applications such as Story Maps to display particular aspects of volcanic areas and have concluded that these tools are suitable for delivering adequate scientific knowledge on topics related to volcanoes (e.g., Antoniou et al., 2018, 2021).

3 METHODOLOGY

3.1 Study Area

The Reykjanes Peninsula in Iceland consists of five major volcanic systems including the Brennisteinsfjöll, the Krýsuvík, the Fagradalsfjall, the Reykjanes, and the Eldey. The Fagradalsfjall volcanic complex is located ~40 km southwest of Reykjavik and covers an area of ~80 km² (Figure 4). The complex was named after the Fagradalsfjall subglacial tuya volcano located in the volcanic system with the same name, morphologically characterized by a flat-top structure and steep-slope hillsides. It has been the least active volcanic system in the Peninsula, and the last recorded eruption was about 6,000 years ago. The 2021 Fagradalsfjall effusive eruption lasted from March to September and marked the end of a long dormancy period in the RP (Global Volcanism Program, 2021; Sæmundsson et al., 2020). The low-intensity volcanic activity produced pahoehoe and a'a basaltic lava flows and minor scoria deposits that emerged from fissure vents within the volcanic system (Figure 5), filling the complex topography cut by nested valleys (Barsotti et al., 2023; Pedersen et al., 2022).

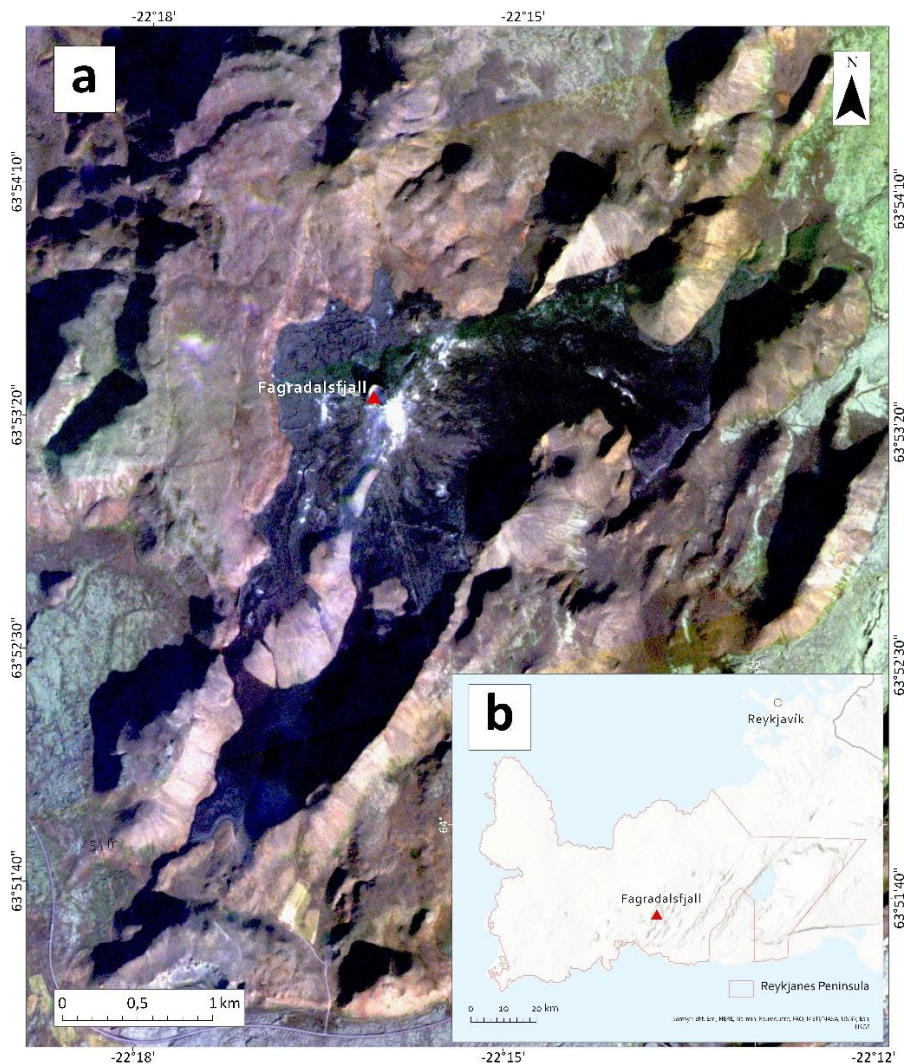


Figure 4: Overview map of the study area. a) Optical image from the 2021 Fagradalsfjall volcanic eruption as for 4 October 2021, Image source: © 2023 Planet Labs, Projection: WGS 84 / UTM zone 27N. b) Overview map of the RP.

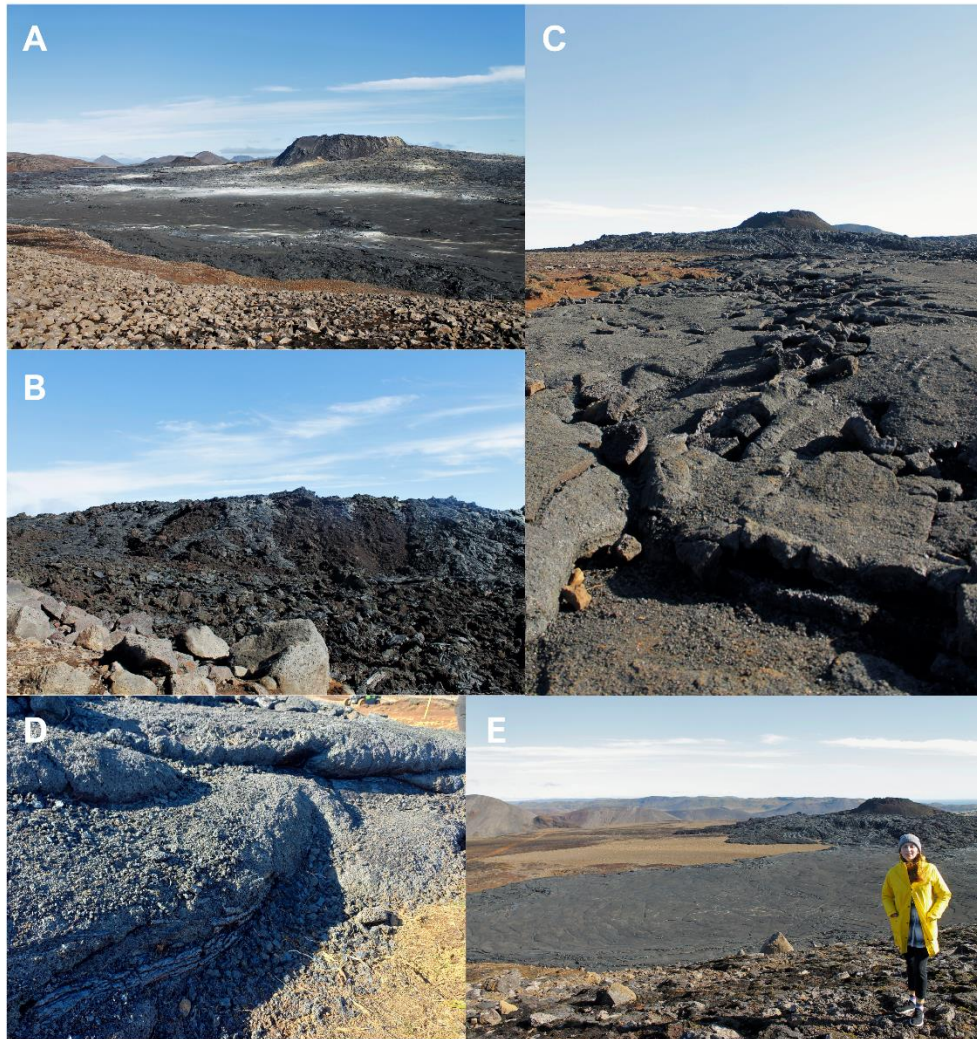


Figure 5: Field pictures. A) Eruptive vent and sulphur alteration in the area. B) Different lava flow textures (pahoehoe and a'a). C) Lava flow path and eruptive vent. D) Lava texture and structures. E) Student in the field.

3.2 Methods

EO data have been useful for lava flow mapping and analysis when applying different remote sensing methodologies. OBIA is among one of the techniques used for geomorphological mapping of volcanic areas, and it has been combined with several types of datasets for the same purpose. Cartography allows the modelling of reality through graphical representations of the spatial dimension of the world; therefore, it is one of the most effective ways to communicate spatial information. This study develops two main research: the first one is the delineation of lava flows from the 2021 Fagradalsfjall eruption using OBIA on Sentinel-1 data, and the second one is the visualisation of the results using cartographic products. The methodological details will be described in subchapters 4 and 5.

3.3 Data

Sentinel 1 data

Sentinel-1 is an active sensor operated by the European Space Agency (ESA) consisting of two polar-orbiting satellites that operate at a wavelength of approximately 5 cm or C-band SAR. Six dual-polarization images of the Sentinel-1 Interferometric Wide Swath (IWS) Level-1 high-resolution Ground Range Detected (GRD) were used for the analysis. All of the products were acquired in descending flight direction. The data were retrieved from [the Alaska Satellite Facility Data Search platform](#).

Elevation data

The Copernicus DEM GLO-30 is a digital surface model of the surface of the Earth available for free and with global coverage provided by the ESA. The data were acquired between 2011 and 2015 within the scope of the TanDEM-X mission. The dataset was retrieved as an embedded source in the SNAP platform and was used for the pre-processing of the Sentinel-1 data. Additionally, the pre and post-eruption DEMs provided by Pedersen et al. (2022) were used for visualisation purposes and were retrieved from an open Zenodo repository in GeoTIFF format: <https://zenodo.org/record/6598466#.ZFO2VnbP02w>.

Table 1 summarises the DEM datasets and the corresponding source.

Table 1: DEMs used during the pre-processing and visualization stages of the study.

Dataset	Source
Copernicus DEM GLO-30	ESA
Pre-eruption Fagradalsfjall DEM	Pedersen et al., 2022
Post-eruption Fagradalsfjall DEM	Pedersen et al., 2022

Vector data

Different vector files displaying the lava paths created as part of the near-real-time monitoring of the 2021 Fagradalsfjall eruption from the work of Pedersen et al. (2022) were retrieved from an open Zenodo repository available online at: <https://zenodo.org/record/6598466#.ZFO2VnbP02w>. The datasets were available in GeoPackage format.

Optical imagery

Sentinel-2 is an active sensor operated by the ESA consisting of two optical satellites that provide multi-spectral imagery within the visible, near-infrared, and short-wave infrared portions of the electromagnetic spectrum. The data were accessed for free through the Copernicus Open Access Hub at: <https://scihub.copernicus.eu/dhus/#/home>. Moreover, PlanetScope 3-band imagery was accessed and retrieved from the Planet Explorer platform at: <https://www.planet.com/explorer> with a license provided by the Planet's Education and Research Program that sponsors students with access to the imagery for research purposes only. The optical datasets were used and processed for the visualisation and storytelling part of this research.

3.4 Software

SNAP

The Sentinel Application Platform is a software distributed by the ESA that provides the architecture for processing and analysing EO data, especially Sentinel products. It is an open-source desktop application.

eCognition Developer

eCognition software is one of the most powerful environments for image feature extraction or change detection developed by Trimble. The tool allows to perform advanced image analysis for different geospatial applications. It is a commercial product, therefore, the eCognition license for this thesis has been provided within the Trimble Innovation Programme (a collaboration between Trimble Geospatial and the Department of Geoinformatics – Z_GIS from the University of Salzburg).

GitHub

GitHub is an open web-based hosting service that allows version control of Git, which is a coding control system that tracks code changes and collaborative coding.

QGIS

QGIS is a GIS desktop software that allows editing, analysis, visualisation, and publishing of geospatial information. The application is free and open source.

Qgis2threejs

Qgis2threejs is a QGIS plugin that allows visualization and web publishing of geospatial data in 3D. The 3D visualization is powered by WebGL and three.js JavaScript technologies.

ArcGIS Pro

ArcGIS Pro is a GIS desktop software developed by ESRI that allows exploring, visualising, analysing, and sharing geospatial data. It is a commercial software; therefore, the license was obtained through the University of Salzburg.

Table 2: Used software with corresponding version and summarised usage.

Software	Version	Usage
SNAP	9.0.0	Pre-processing of the Sentinel-1 imagery
eCognition Developer	10.3	Image segmentation and lava flows classification
ArcGIS Pro	3.0.2	Vector data processing, validation, visualisation
QGIS	3.22.2	Vector data processing, visualisation
Qgis2threejs	2.7.1	Creation of the 3D web map application

3.5 Processing procedure

Figure 6 explains the key steps performed for the development of the present study. Initially, the data collection of Sentinel-1, Sentinel-2, PlanetScope imagery, DEMs of the area, and their corresponding pre-processing was conducted using ArcGIS Pro, QGIS, and SNAP software. After processing the datasets, the OBIA methodology which includes three main steps (multiresolution segmentation, knowledge-based ruleset classification, and refinement) can be applied to the Sentinel-1 data to delineate the lava flows from the 2021 Fagradalsfjall eruption over time. The results are then compared with the reference data available in the literature by performing an accuracy assessment. The outputs, the models, and the optical imagery processed for the study area are used to create static maps and a 3D web map application that includes an animation to visualise the results interactively, allowing experts and enthusiasts to explore the lava flow outlines obtained for the volcanic eruption and the story behind it.

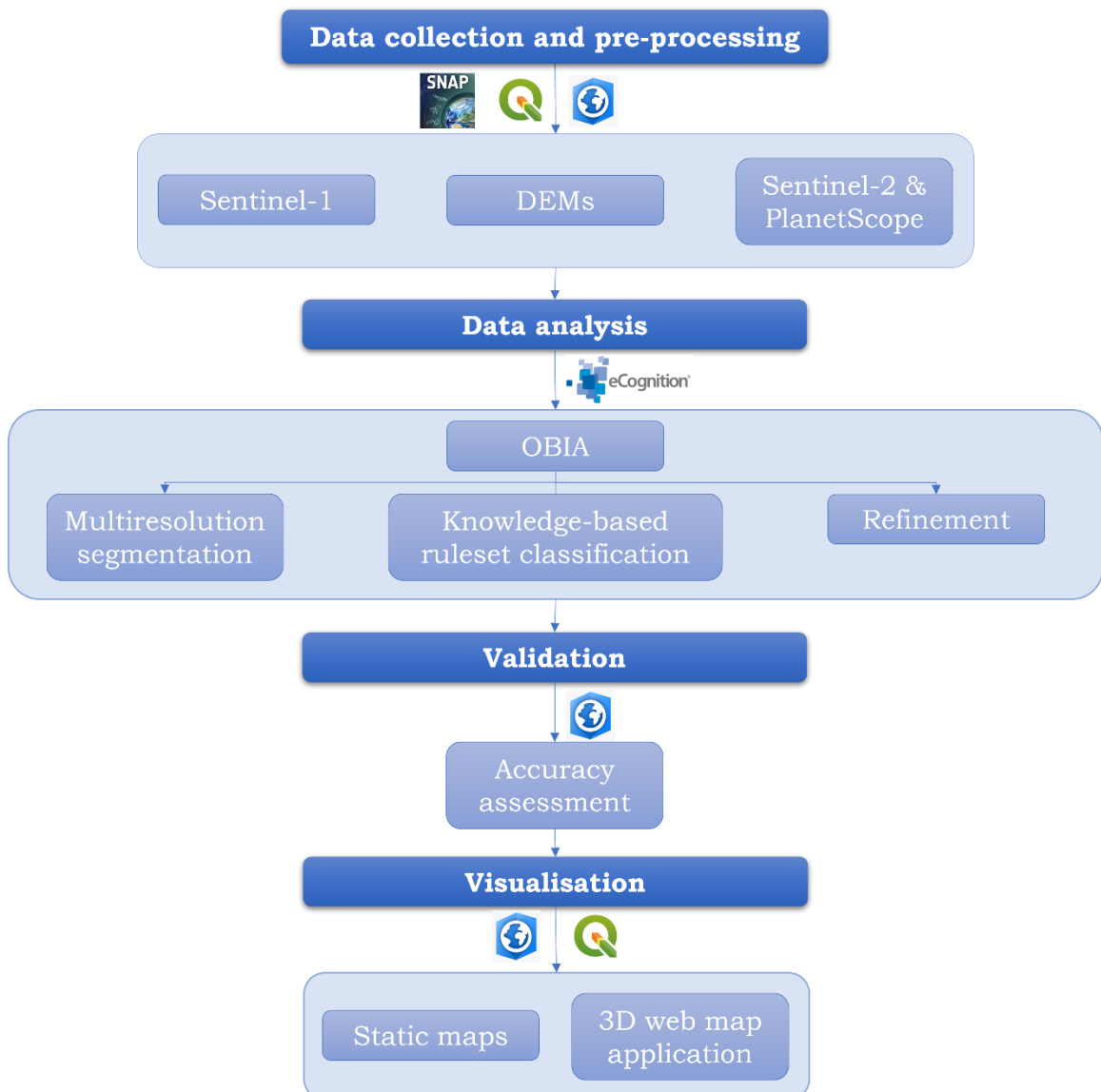


Figure 6: Summarised research workflow and processing steps.

4 LAVA FLOW MAPPING

In this chapter, the methodology and processing steps associated with the lava flow mapping of the 2021 Fagradalsfjall eruption are documented and discussed in detail. It has been divided into three subchapters that describe the main stages followed during the development of the analysis. A step-by-step explanation for the pre-processing, delineation, and validation phases is provided, along with technical specifications and a discussion of the decision-making process.

4.1 Data collection and pre-processing

Pre, syn and post-event Sentinel-1 data of the 2021 Fagradalsfjall volcano were retrieved from the Alaska Satellite Facility Data Search Platform. Sentinel-1B with C-band penetration and dual polarisation IWS GDR products were used for the analysis and delineation. Table 3 summarises the date and the corresponding phase of the eruption associated with each image. Once the data were identified and collected, they had to be processed for the information of interest to be extracted. Figure 7 shows the resulting images after applying the pre-processing steps to the Sentinel-1 data. Data pre-processing of Sentinel-1 data in SNAP software included different steps and followed the workflow suggested by (Filipponi, 2019):

- Orbit file application: The orbit file contains relevant information related to the metadata of the image product that provides an accurate satellite position and ensures that spatial co-registration processes are successful. The orbit file was automatically downloaded from SNAP software and then it was applied to the SAR image.
- Radiometric calibration: This process converts the digital pixel values of the SAR image so that they represent the real backscattering of the surface, allowing the quantitative use of the SAR data. The calibration was performed in sigma nought, gamma, and beta values. This step is important when comparing images acquired from the same sensor at separate times or in different modes.
- Radiometric terrain flattening: This process was applied to correct radiometric distortions in the SAR image that are related to the topography of the scene. This algorithm required the beta input generated from the radiometric calibration. This step was useful to reduce the effects of the side-looking nature of the SAR sensor which causes objects facing the sensor to appear unnaturally brighter and objects facing away from the sensor to appear unnaturally darker.
- Refined Lee speckle noise filtering: Speckle filtering was applied to reduce the "salt and pepper" effect or granular noise that appears in SAR imagery due to wave interference caused by scatterers reflected by several features. The Refined Lee filter was selected because it increased the image quality without losing spatial resolution and because of its ability to preserve texture information.
- Range Doppler terrain correction: The terrain correction improves the geometric representation of the image by compensating the effects of the side-looking geometry of the SAR sensors including foreshortening and shadows. The algorithm used the Copernicus DEM GLO-30 (Table 1) to correct the location of each pixel and to orthorectify the image, resulting in precise geolocation information of the

SAR scene. The images were resampled to match the grid reference of the UTM 27N coordinate system for the studied region in Iceland.

- Conversion to decibel scale: Using a logarithmic transformation, the backscatter coefficients were converted to decibel scale (dB) .

Table 3: Sentinel-1 data used to semi-automatically delineate and map the lava flow from the Fagradalsfjall 2021 eruption.

Date	Event
22 August 2020	Pre-eruption
31 March 2021	Syn-event (Phase 1)
12 April 2021	Syn-event (Phase 2)
18 May 2021	Syn-event (Phase 3)
29 July 2021	Syn-event (Phase 4)
27 September 2021	Post-eruption

Additionally, geometric distortions in SAR images can cause misalignments among satellite images acquired at consecutive times, which results in impaired change detection analysis. To reduce the effects of misalignments, the images were co-registered in temporal stacks using SNAP software. The purpose of the co-registration process was to visualise the motion or the changes occurring from one image to another and then use the stacks to apply the corresponding analysis for delineating the lava flows of the 2021 Fagradalsfjall volcano using OBIA.

Pairs of consecutive images were selected to create co-registered stacks for each eruptive phase as described in Table 4. For each stack, the total amount of bands was 16, eight representing the first image date and eight representing the second image date. All of the bands were conserved to test which of them could be useful for the segmentation and classification of the images when applying the OBIA methodology. Table 5 briefly describes the information contained in each band of the co-registered stacks.

Table 4: Dates of the co-registered stacks for each eruptive phase.

Dates	Stack
22/08/2021 - 31/03/2021	Phase 1
31/03/2021 - 12/04/2021	Phase 2
12/04/2021 - 18/05/2021	Phase 3
18/05/2021 - 29/07/2021	Phase 4
29/07/2021 - 27/09/2021	Post-eruption

Figure 8 displays the resulting co-registered stacks for the pairs of consecutive images (Table 4) used for detecting the changes in each eruptive phase of the Fagradalsfjall volcano. The bands with co-polarised signal (VV, HH) show less contrast than the bands with cross-polarised signal (VH, HV); hence, the gamma calibration with dual polarization VH converted to dB was used for visualisation purposes because it displayed the best

contrast. Both the gamma and the sigma nought calibration allow to easily recognize the changes between images. The Red Green Blue (RGB) band combination used for the stacks follows:

- Red: Band 13 or Band 14.
- Green: Band 13 or Band 14.
- Blue: Band 5 or Band 6.

Table 5: Information contained on each band of the co-registered stacks.

Band	Description
Band 1	Linear Gamma_VH backscatter value for the first date image.
Band 2	Linear Sigma_VH backscatter value for the first date image.
Band 3	Linear Gamma_VV backscatter value for the first date image.
Band 4	Linear Sigma_VV backscatter value for the first date image.
Band 5	Gamma_VH_dB backscatter value for the first date image in dB.
Band 6	Sigma_VH_dB backscatter value for the first date image in dB.
Band 7	Gamma_VV_dB backscatter value for the first date image in dB.
Band 8	Sigma_VV_dB backscatter value for the first date image in dB.
Band 9	Linear Gamma_VH backscatter value for the second date image.
Band 10	Linear Sigma_VH backscatter value for the second date image.
Band 11	Linear Gamma_VV backscatter value for the second date image.
Band 12	Linear Sigma_VV backscatter value for the second date image.
Band 13	Gamma_VH_dB backscatter value for the second date image in dB.
Band 14	Sigma_VH_dB backscatter value for the second date image in dB.
Band 15	Gamma_VV_dB backscatter value for the second date image in dB.
Band 16	Sigma_VV_dB backscatter value for the second date image in dB.

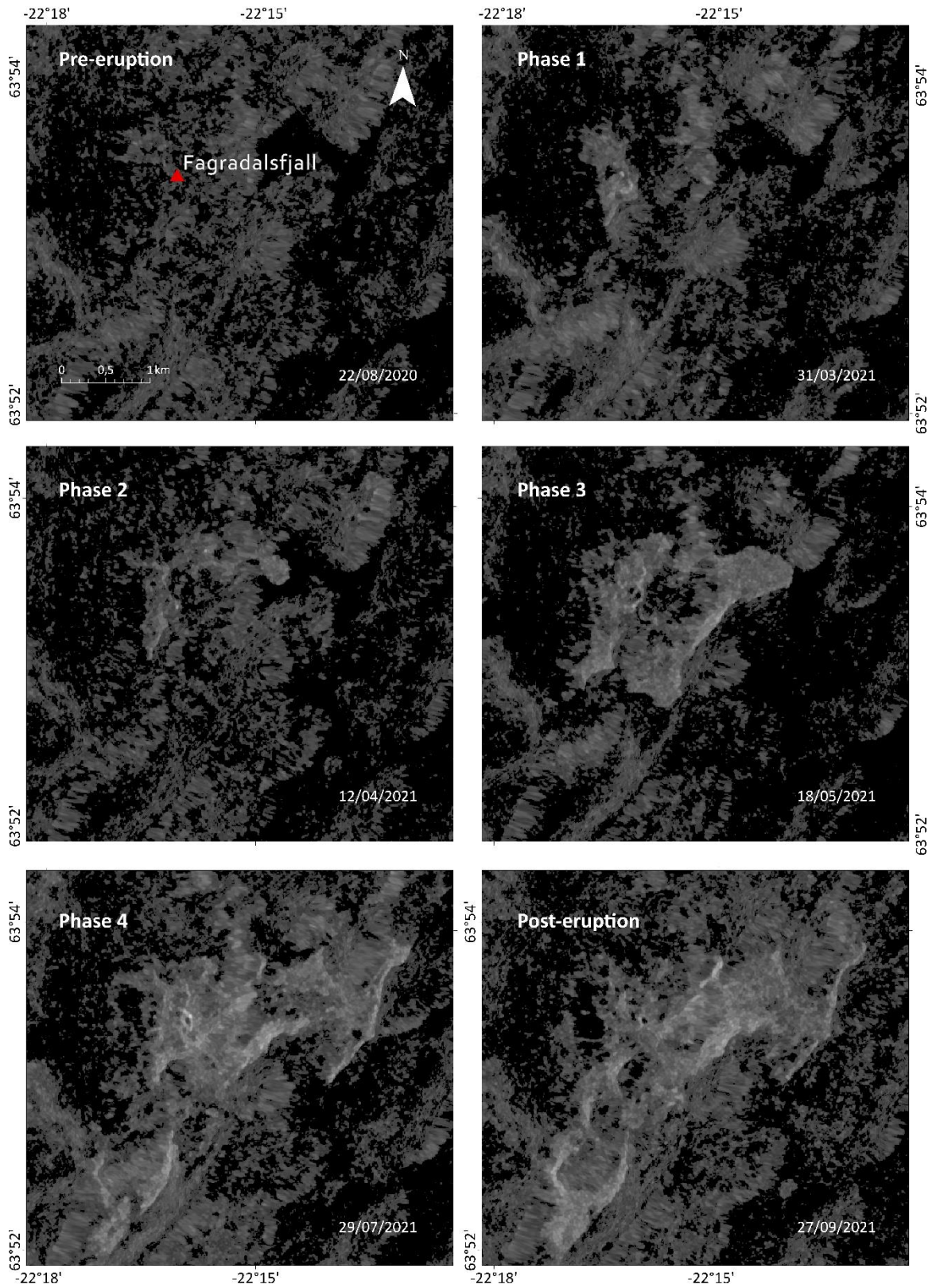


Figure 7: Sentinel-1 imagery after applying pre-processing steps.

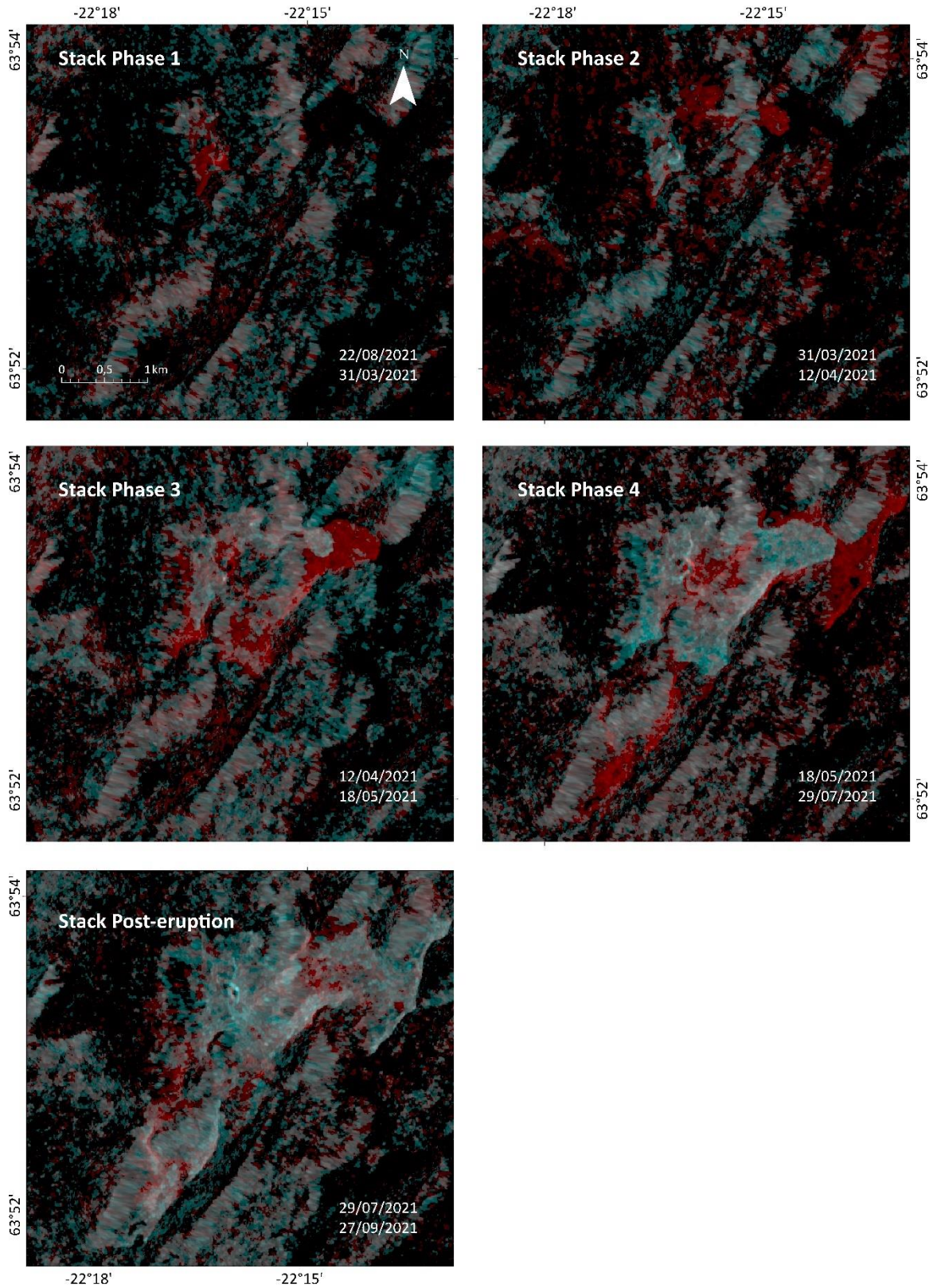


Figure 8: Sentinel-1 imagery after creating co-registered stacks for each eruptive phase.

4.2 Lava flow delineation

OBIA was selected for the lava flow delineation because the image analysis can be done not only considering the value of individual pixels, which neglects spatial concepts but also according to additional contextual properties obtained by grouping pixels (Blaschke, 2010). Additionally, pixel-based approaches applied on fine-resolution data can be affected by noise (salt-and-pepper effect) caused due to disperse classification of individual cells and because of the high spectral variation within classes, while object-based analysis applied on high spatial resolution data provides more homogeneous objects and classification (Blaschke, 2010).

The lava flows of the 2021 Fagradalsfjall eruption were mapped using OBIA and the analysis was performed using eCognition (©Trimble) software. OBIA consists of two major steps: segmentation and classification. Initially, a multiresolution segmentation algorithm was applied to create homogeneous objects by grouping pixels with similar characteristics. For the subsequent classification, some spatial, geometric, and textural properties of the geographic objects were used as inputs in a knowledge-based classification ruleset. Different segmentation parameters and bands were used for the segmentation of each eruptive phase and further refinement of the classification was performed through merging algorithms and considering spatial relations between objects, before validating the results. Visual assessment of the intermediate results and human-driven trial and error tests were used to determine the threshold values for the classification. Then, the results were exported in GeoJSON format and post-processed in QGIS and ArcGIS software.

The multi-resolution segmentation step in eCognition required the configuration of different parameters including scale parameter, shape, and compactness. The algorithm clusters neighbour pixels into single image objects based on homogeneity criteria which considers spectral and shape properties of the features. Therefore, the criterion determines how homogeneous or heterogeneous an image is. Usually, to find the optimal parametrisation it is necessary to perform trial and error testing to achieve the best degree of object homogeneity.

The shape parameter can vary from 0.1 to 0.9 and determines the influence of shape against colour in the segmentation. Therefore, if the value is fixed to 0.3, the weight of the shape will take the same value and the colour weight will be 0.7. The compactness criterion will compare how compact or smooth an object will be, again varying from 0.1 to 0.9. The sum of shape and compactness criteria must be one (Trimble Germany GmbH, 2022). The scale parameter controls the size of the image objects. The correct selection of the scale parameter will influence the classification results and the accuracy of the analysis. Assigning a small scale parameter value will create smaller features and is more suitable for extracting small features, whereas a high scale parameter will create larger segments allowing extraction of bigger features. The more pixels enclosed within each segment; the more information is available for the classification process. However, an incorrect configuration of the scale parameter in high-resolution data can limit its effectiveness and can lead to over or under segmentation because of the level of detail displayed by the image. Over-segmentation can make the classification process more difficult because the variation within the same class increases and on the other hand,

under-segmentation can lead to loss of detail making the classification more inaccurate (Robb et al., 2015). Ideally, the objects should have the same size, or a smaller size compared to the features to be classified because over-segmentation can be fixed by merging algorithms using contextual information of neighbouring objects.

Phase 1

The changes in phase 1 of the eruption were delineated using the stack of the pre-eruption and the syn-eruption phase 1 (Table 4). The main threshold values used for the classification including mean value and standard deviation were extracted from a layer created using the layer arithmetic tool in eCognition, which was called the subtraction layer (SL). The SL is the subtraction between Band 14 and Band 6 (Table 5) and it contained the backscattering values in decibel scale of the corresponding dates of the stack, resulting in a difference value that displays how much the segment change from the pre-event to the phase 1. For the refinement, the relative border to lava defines how much of a segment border in the image is shared with a neighbouring segment classified as lava. The value was set to 0 meaning that there is no border length shared with the other lava segments, classifying these objects as “NoLava”.

The parametrisation of the segmentation and the threshold values used for the classification and the refinement of phase 1 are summarised in Figure 9. Figure 10 shows a preview of the eCognition resulting segmentation and classification for phase 1.

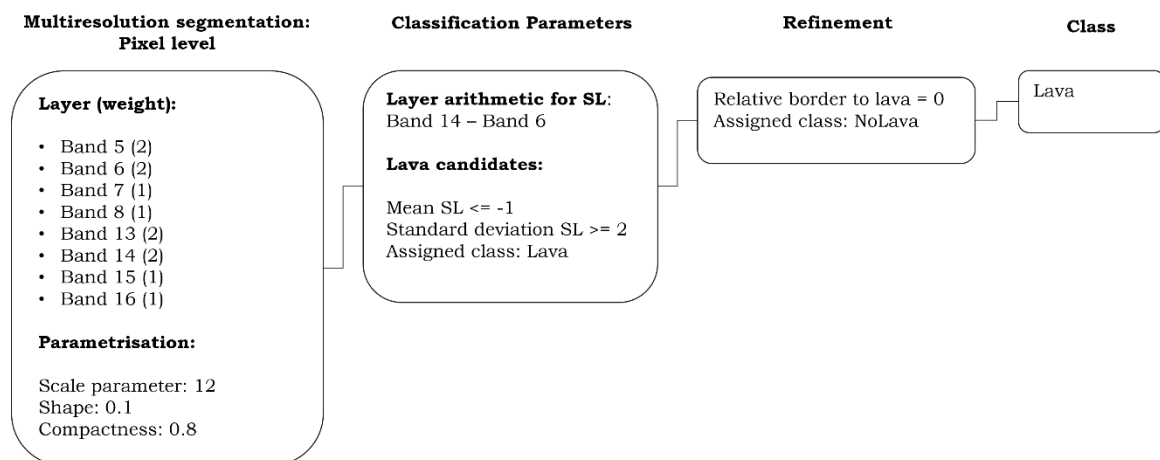


Figure 9: Detailed workflow used for the delineation of the Phase 1 of the eruption.

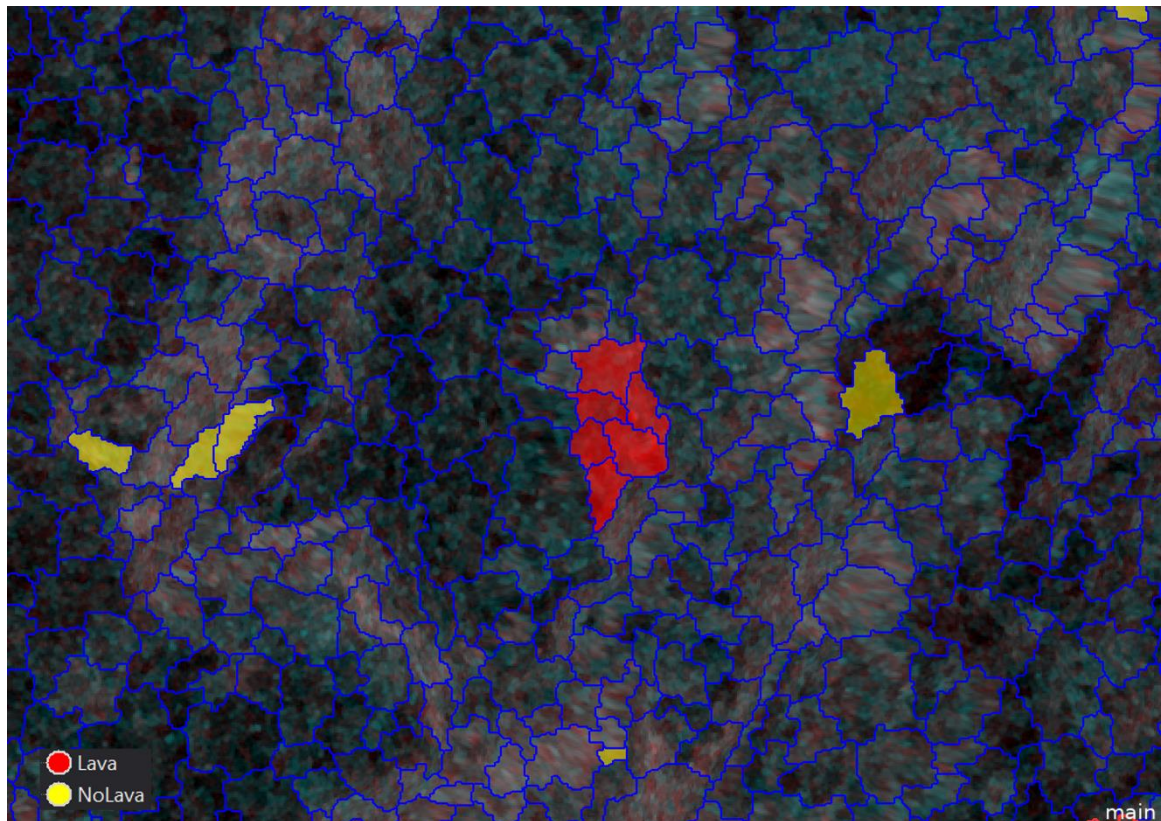


Figure 10: Preview of the segmentation and classification obtained for the Phase 1 in eCognition. The blue polygons represent the unclassified segments in the scene.

Phase 2

The changes in phase 2 of the eruption were delineated using the stack of the syn-eruption phase 1 and phase 2 images (Table 4). For the multiresolution segmentation, a thematic layer containing the classified area from phase 1 was considered to maintain the integrity of the delineation through time. In the classification, the minimum overlap percentage feature was used to create an overlapping value with the lava flows that were detected in phase 1, excluding them for the classification. The main threshold values used for the classification of the lava were extracted from the SL which displayed the difference between Band 13 and Band 5 (Table 5), and it contained the backscattering values in decibel scale of the corresponding dates of the stack. Therefore, the SL is a difference value that displays how much the segment changed from phase 1 to phase 2. The mean value of Band 13 was also used for the classification because the backscattering values of the lava were very strong compared to the surrounding areas, making it useful for the extraction. For the refinement, the eCognition merging algorithm was used to merge the segments with very small area. Additionally, the relative border feature was used to exclude large segments that did not correspond to the lava class.

The parametrisation of the segmentation and the threshold values used for the classification and the refinement of phase 2 are summarised in Figure 11. Figure 12 shows a preview of the eCognition resulting segmentation and classification for phase 2.

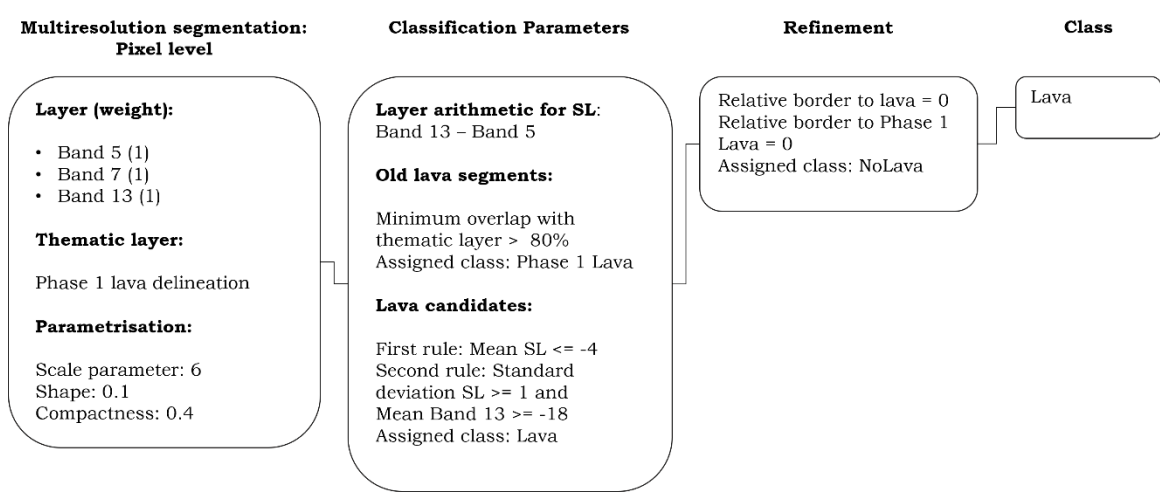


Figure 11: Detailed workflow used for the delineation of the Phase 2 of the eruption.

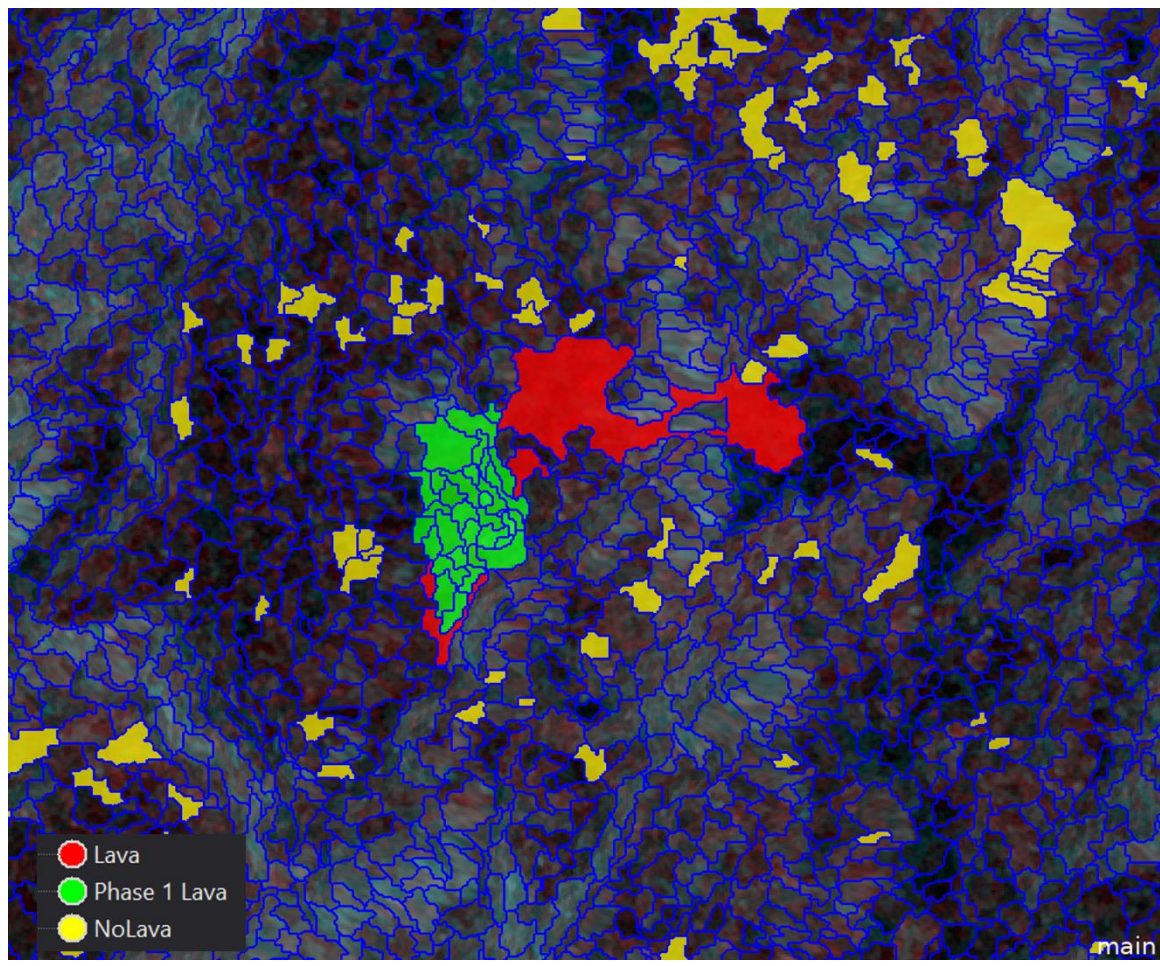


Figure 12: Preview of the segmentation and classification obtained for the Phase 2 in eCognition. The blue polygons represent the unclassified segments in the scene.

Phase 3

The changes in phase 3 of the eruption were delineated using the stack of the syn-eruptive phase 2 and phase 3 images (Table 4). For the multiresolution segmentation, the thematic layers containing the classified area from phase 1 and phase 2 were considered to maintain the integrity of the delineation through time. In the classification, the minimum overlap percentage feature was used to create an overlapping value with the lava flows that were detected in phase 1 and phase 2, excluding them for the classification of the phase 3 lavas. The main threshold values used for the classification of the lava were extracted from two different SL, one displaying the difference between Band 13 and Band 5, and the other one showing the difference between Band 14 and Band 6 (Table 5). Both of the SL contained the backscattering values in decibel scale for the corresponding dates of the stack and represent how much the segments changed from phase 2 to phase 3. The mean values of Band 5 and Band 6 were also used for the classification because they displayed the strong backscattering values of the lava during the phase 3 compared to the surrounding areas. For the refinement, the eCognition merging algorithm was used to merge segments with very small areas that prevented their correct classification due to the variability of the values in few pixels. The merging algorithms used combinations of conditions that included the area of the segments and the mean SL values. Finally, the relative border feature was used for refinement as it allowed to exclude large segments that did not correspond to the lava class.

The parametrisation of the segmentation and the threshold values used for the classification and the refinement of phase 3 are summarised in Figure 13. Figure 14 shows a preview of the eCognition resulting segmentation and classification for phase 3.

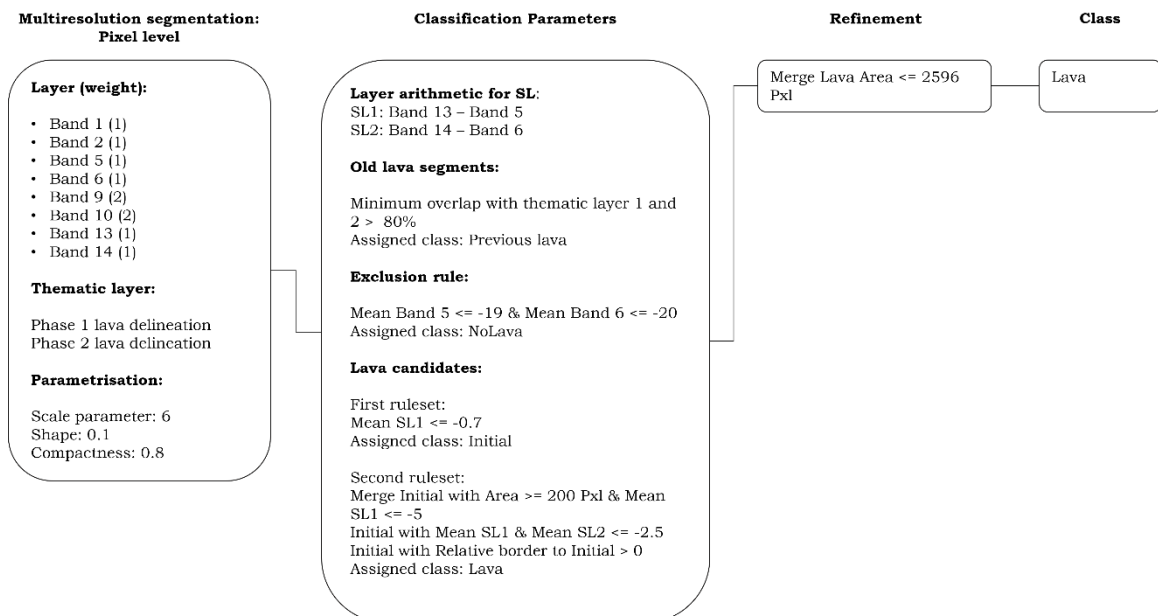


Figure 13: Detailed workflow used for the delineation of the Phase 3 of the eruption.

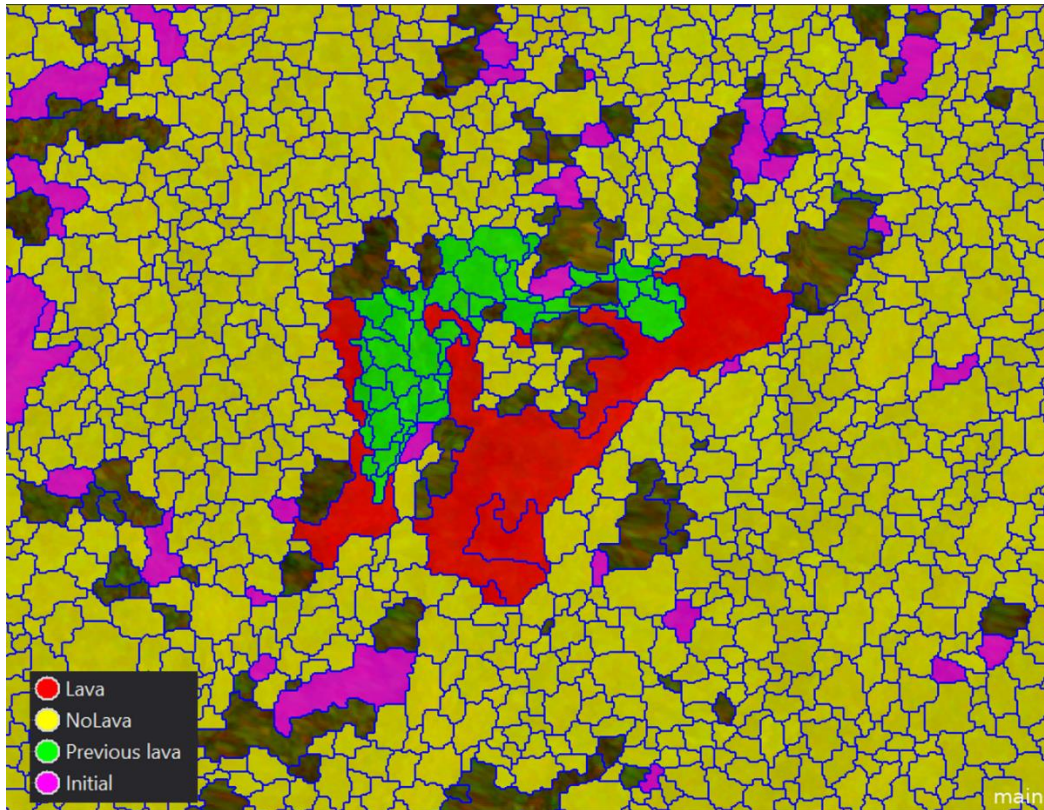


Figure 14: Preview of the segmentation and classification obtained for the Phase 3 in eCognition. The blue polygons represent the unclassified segments in the scene.

Phase 4

The changes in phase 4 of the eruption were delineated using the stack of the syn-eruptive phase 3 and phase 4 images (Table 4). For the multiresolution segmentation, the thematic layers containing the classified area from phase 1, phase 2, and phase 3 were considered to maintain the integrity of the delineation through time. In the classification, the minimum overlap percentage feature was used to create an overlapping value with the lava flows that were detected in phase 1, phase 2, and phase 3, excluding them for the classification of the phase 4 lavas. The main threshold values used for the classification of the lava were extracted from a SL which displayed the difference between Band 14 and Band 6 (Table 5). The SL contained the backscattering values in decibel scale for the corresponding dates of the stack and represent how much the segments changed from phase 3 phase 4. For the refinement, the eCognition merging algorithm was used to merge segments with very small areas. A geometry feature describing the symmetry of the object shape was used during the refinement process to exclude objects from the lava class. Finally, the relative border feature was used for refinement as it allowed to exclude segments that did not correspond to the lava flow.

The parametrisation of the segmentation and the threshold values used for the classification and the refinement of phase 4 are summarised in Figure 15. Figure 16 shows a preview of the eCognition resulting segmentation and classification for phase 4.

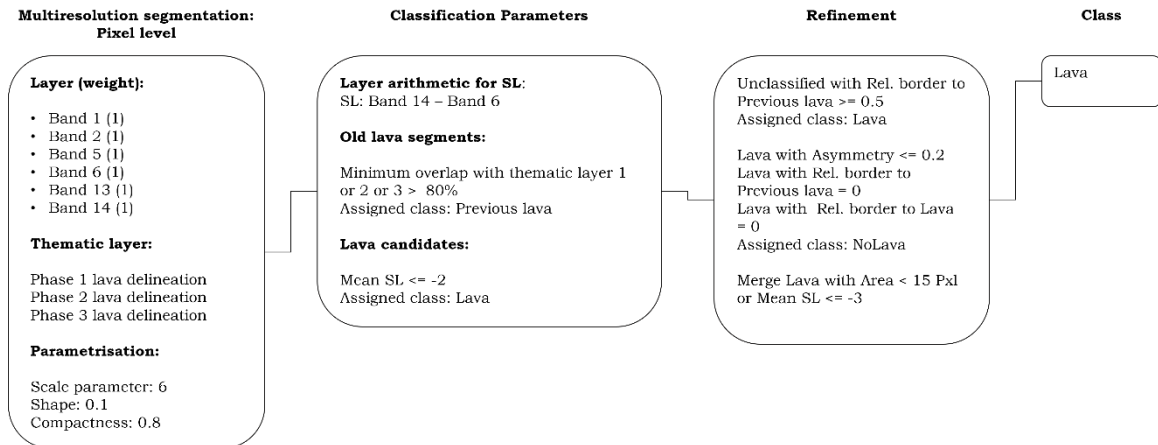


Figure 15: Detailed workflow used for the delineation of the Phase 4 of the eruption.

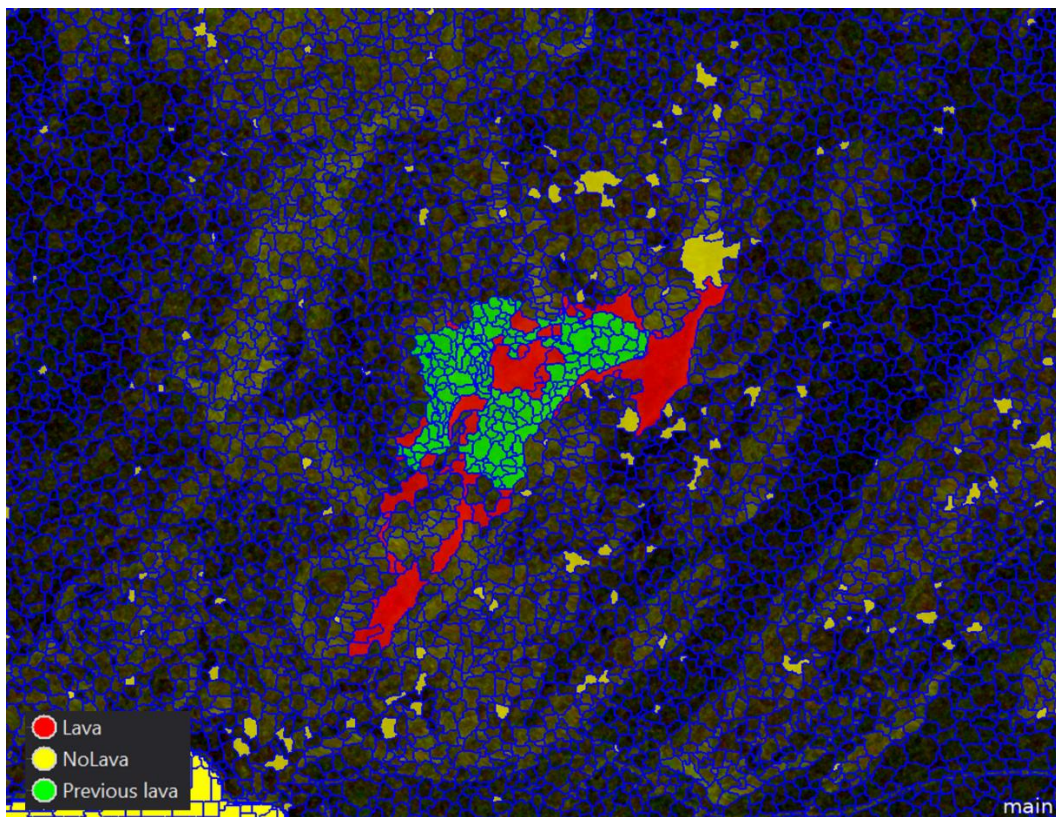


Figure 16: Preview of the segmentation and classification obtained for the Phase 4 in eCognition. The blue polygons represent the unclassified segments in the scene.

Post-eruption

The changes in phase 5 of the eruption were delineated using the stack of the syn-eruptive phase 4 and the post-eruption images (Table 4). For the multiresolution segmentation, the thematic layers containing the classified area from phase 1, phase 2, phase 3, and phase 4 were considered to maintain the integrity of the delineation through time. In the classification, the minimum overlap percentage feature was used to create an overlapping value with the lava flows that were detected in phase 1, phase 2, phase 3, and phase 4 excluding them for the classification of the post-eruption lava field. The main threshold values used for the classification of the lava were extracted from a SL which displayed

the difference between Band 14 and Band 6 (Table 5). The SL contained the backscattering values in decibel scale for the corresponding dates of the stack and represent how much the segments changed from phase 4 to the post-eruption. The mean values of Band 6 were also used for the classification because it displayed a strong backscattering value of the lava flow for the post-eruption image. For the refinement, the eCognition merging algorithm was used to merge segments with small areas, and the relative border feature was used for excluding segments that did not correspond to the lava flow. The parametrisation of the segmentation and the threshold values used for the classification and the refinement of the post-eruption are summarised in Figure 17. Figure 18 shows a preview of the eCognition resulting segmentation and classification for the post-eruption.

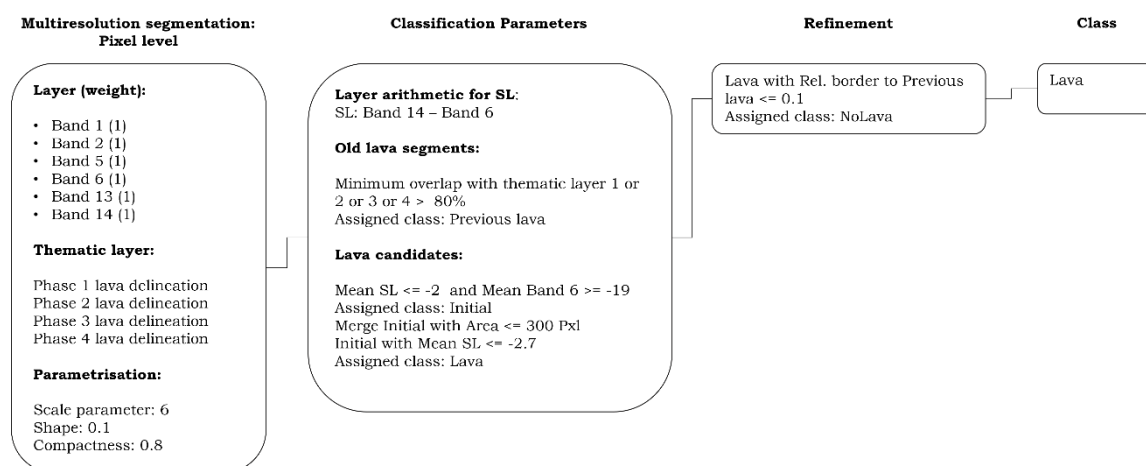


Figure 17: Detailed workflow used for the delineation of the Post-eruption.

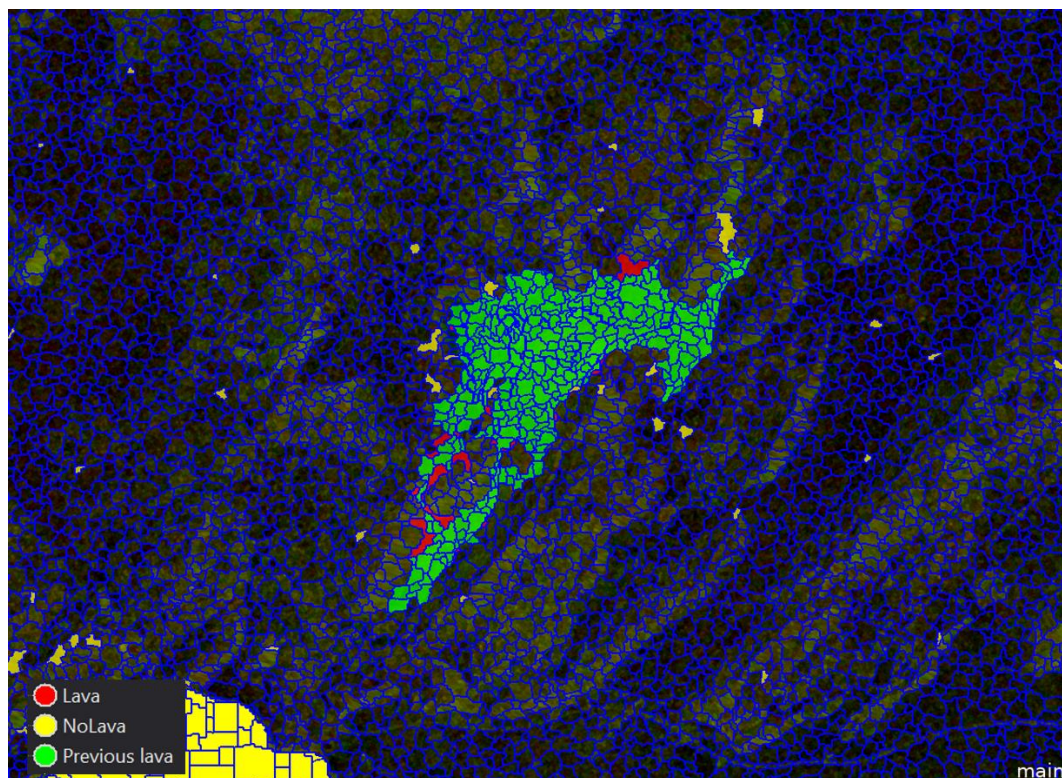


Figure 18: Preview of the segmentation and classification obtained for the post-eruption in eCognition. The blue polygons represent the unclassified segments in the scene.

4.3 Validation

The accuracy assessment measured and compared the overlapping area between the results obtained with OBIA and the lava outlines calculated in Pedersen et al. (2022). Orthophotos, DEMs, and thickness maps were generated from aerial photogrammetric surveys and Pleiades stereo images to manually map the lava flows and calculate the lava volume and effusion rates of the 2021 Fagradalsfjall eruption in Pedersen et al. (2022). Table 6 shows the datasets selected as ground data to compare with the results obtained with the OBIA technique applied to SAR data. Most of the selected reference dates exactly match the dates used for the lava delineation with OBIA except for the post-eruption.

Congalton (1991) discusses descriptive and analytical techniques for assessing the accuracy of classifications on remote sensing imagery. A descriptive technique can assess the classification by comparing the total correct classified area and the classification results. The overlapping area represents the area that was correctly classified. The producer's accuracy is the ratio between the overlapping area and the OBIA classification, which represents errors of inclusion. The user's accuracy is the ratio between the overlapping area and the reference data, which represents errors of exclusion. Table 7 summarises the obtained areas for each method and each event, the corresponding overlapping area, and the accuracies obtained.

Table 6: Lava flow outlines used as reference for the accuracy assessment (source: Pedersen et al., 2022)

Dataset	Associated date	Associated event
Outline_20210331_1210_A6D_Pedersen_et al2022.gpkg	31 March 2021	Phase 1
Outline_20210412_1210_A6D_Pedersen_et al2022.gpkg	12 April 2021	Phase 2
Outline_20210518_1730_A6D_Pedersen_et al2022.gpkg	18 May 2021	Phase 3
Outline_20210727_1000_A6D_Pedersen_et al2022.gpkg	27 July 2021	Phase 4
Outline_20210930_1420_A6D_Pedersen_et al2022.gpkg	30 September 2021	Post-eruption

Table 7: OBIA and orthophotos (Pedersen et al., 2022) mapped area, difference in mapping results, area of overlapping, and accuracies calculated for each event.

Event	OBIA (km ²)	Orthophotos (km ²)	Difference (%)	Overlap (km ²)	Producers Accuracy (%)	User's Accuracy (%)
Phase 1	0,32	0,30	6,74	0,26	81,62	87,12
Phase 2	0,73	0,74	-2,12	0,64	88,45	86,58
Phase 3	2,07	2,06	0,35	1,89	91,59	91,91
Phase 4	4,10	4,28	-4,37	3,80	92,83	88,78
Post-eruption	4,32	4,85	-10,82	4,15	96,01	85,61

5 LAVA FLOWS VISUALISATION

In this chapter, the methodology and processing steps associated with the lava flows visualisation of the 2021 Fagradalsfjall eruption are described in detail. It has been divided into two subchapters that describe the main stages followed for visualising the results obtained in Chapter 4. A step-by-step explanation for the pre-processing and web mapping processes is provided.

5.1 Pre-processing

The pre- and post-eruption Fagradalsfjall DEMs (Table 1) provided freely by Pedersen et al. (2022) were used as elevation surfaces for creating a 3D static map and a 3D interactive Web Map application. The DEMs were clipped to the study area extent, and the gaps were filled using QGIS tools. Figure 19 shows the pre- and post-event elevation models of the study area retrieved from Pedersen et al. (2022).

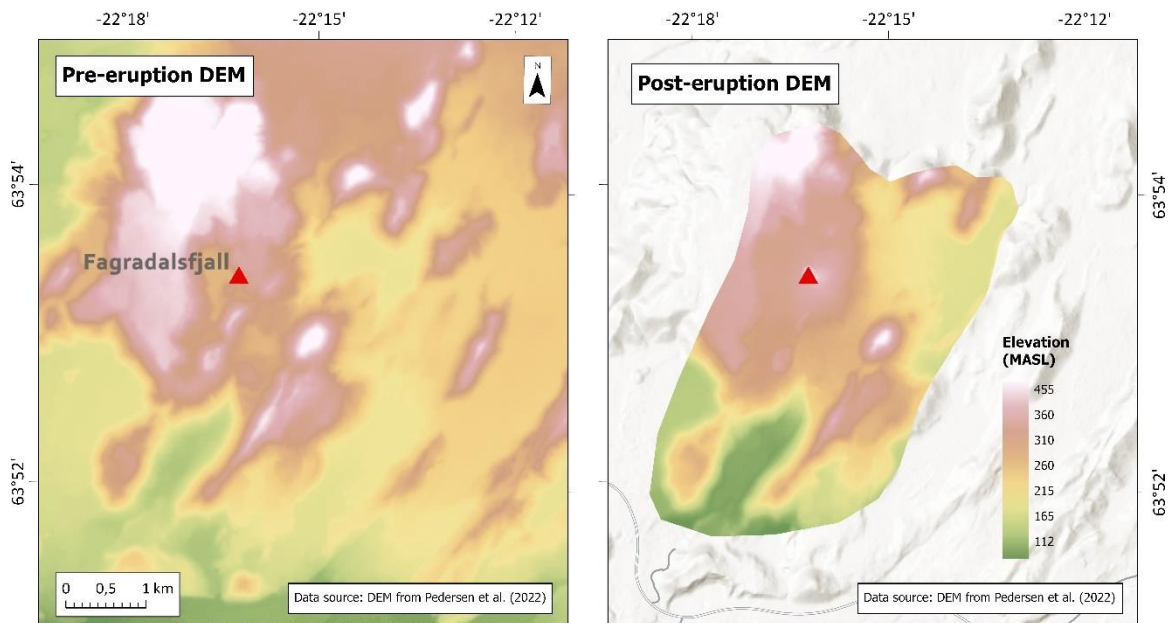


Figure 19: Pre- and post-eruption DEMs retrieved from Pedersen et al. (2022).

A post-eruption PlanetScope image as of 04.10.2021 was used to texture the elevation surfaces in the visualisations. The symbology of the image was configured to be visualise using a standard deviation stretch of 2 and a gamma value of 1,5.

The lava flow paths obtained in Chapter 4 were processed in QGIS software to merge all the features of each phase into single features for better management of the data. The features were then converted to multipatch using the “Interpolate Polygon to Multipatch” tool in ArcGIS Pro to assign the elevation values of the post-eruption Fagradalsfjall DEM to the lava flow polygons and project them correctly in the 3D models.

All of the layers were projected to WGS 84 / UTM zone 27N to display the data with as little distortion as possible and to maintain the geographic reference system integrity of the visualisations.

5.2 Visualisation

3D Web Map application

The Qgis2threejs plugin was installed in QGIS, and it allowed the creation of a 3D scene arranging the lava flow multipatches on top of the elevation surfaces that could be exported directly to the web. The final export consisted of a HyperText Markup Language (HTML) and several JavaScript (JS) and Cascading Style Sheets (CSS) files. Additionally, the plugin allowed the creation of an animation of the scene accompanied by multimedia elements and text that allowed the visualisation to be presented in the form of a story. Besides, the design of the final application was customised using the native files provided by the plugin and it was uploaded to GitHub and configured as a public website. The step-by-step procedure used to create the animation follows:

1. Load elevation surface, vector, and raster layers in QGIS, perform pre-processing and style them accordingly.
2. Open the Qgis2threejs exporter from the QGIS toolbar. The “Layers” panel to the left side of the window displays the map layers that are currently opened with the QGIS project and that are available to add in the 3D scene. Select the elevation layers to add them to the scene. Figure 20 shows the preview of the 3D scene after adding the DEMs. Additionally, the geometry, material, and tiles of the layers can be configured.

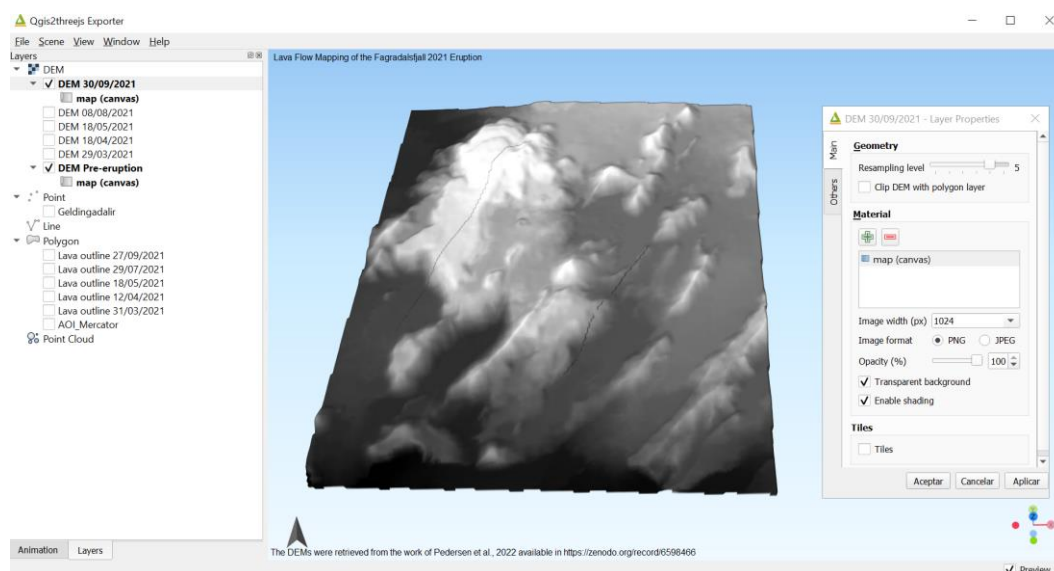


Figure 20: Qgis2threejs preview window displaying the elevation surfaces and their configuration in the 3D scene.

- Apply texture to the elevation surfaces using the material configuration available in the “Layer Properties” window. The post-event image from PlanetScope was used as the overlaying texture of the scene because of the high resolution of the data which allows a better rendering. Additionally, the lava outlines were loaded into the scene and configured with an “Addend” of 10 to be displayed correctly on top of the elevation surface (Figure 21).

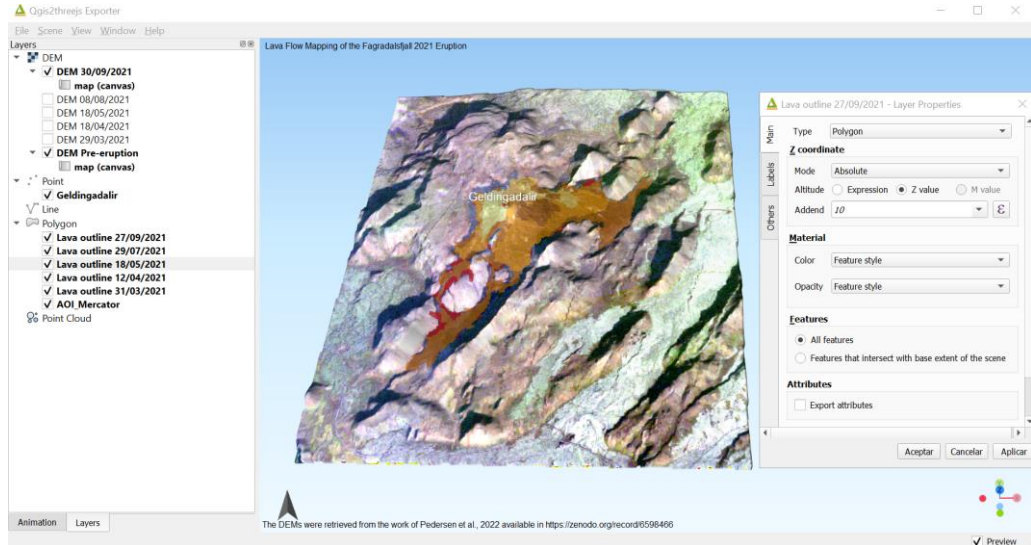


Figure 21: Qgis2threejs preview window displaying the raster and vector overlaying layers and their configuration in the 3D scene.

- Animation and narratives were added to the scene from the “Animation” left-side panel in the plugin exporter. Seven keyframes were created and the narrative content and multimedia support were added to each of the keyframes to display a story while the scene moves. The easing and duration of the keyframes were configured in the “Camera Motion” window.

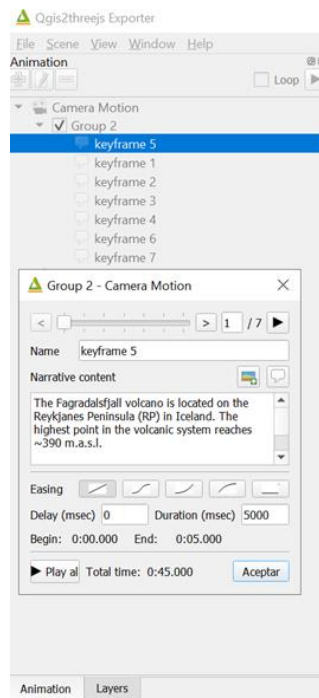


Figure 22: Qgis2threejs animation panel and the keyframes configuration window.

- The scene and the animation were exported to the web using the “3D Viewer with dat-gui panel” template because it allows the user to interact with layers by adjusting their visibility and opacity in the web scene. The settings for the camera were configured to display a perspective camera for which the closer the object, the bigger it renders and the farther the object, the smaller it renders.

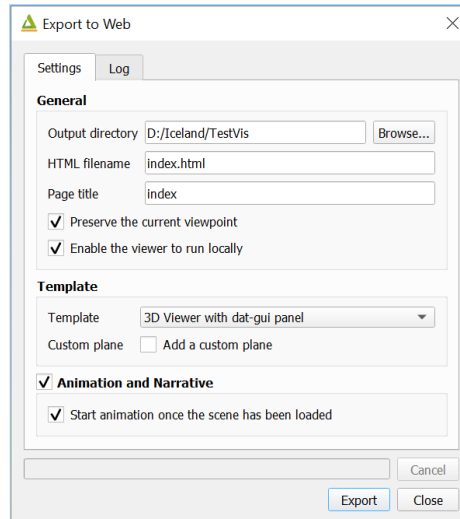


Figure 23: Qgis2threejs export settings used for the 3D web application of the 2021 Fagradalsfjall eruption.

Static Map

A 3D static map visualising the lava flows on top of the elevation surfaces was created using an ArcGIS Pro local scene, which allows three-dimensional representations of spatial data.

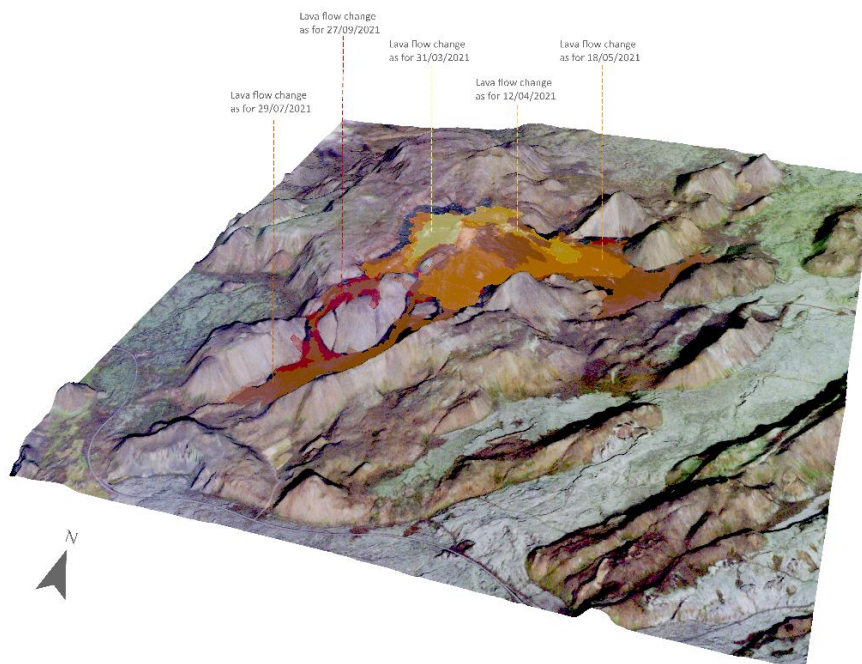


Figure 24: 3D static map visualising the delineated lava flows.

6 RESULTS

The objectives of this project were to delineate the lava flow of the 2021 Fagradalsfjall eruption, to compare the delineation with existing reference data, and to visualise the results interactively. Two main research sections described in detail the methodology used to achieve these goals, leading to relevant findings. The results section presents a summary of the findings. The lava flow mapping results are comprised in the form of time-series maps and figures that showcase the changes detected during the eruption and the visualisation results consist of the web application itself and the 3D static map.

6.1 Lava flow mapping results

The results of the lava flow mapping using OBIA on radar data are shown in Figure 25. The pre-eruption image shows the study area before the lava flows started to infill the Geldingadallir valley, and it was used as an initial reference for the identification of the changes throughout the eruption. The figure shows the lava flow extent classified for each phase after refinement and post-processing.

The resulting area for the delineation of phase 1 was 0,32 km² (Table 7). The extent of the lavas infilled mainly the north-western part of the Geldingadallir valley and the range of elevations that it covered varied from 245 up to 317 meters above sea level (MASL). For phase 2, the lava continued its course to the northeast, accumulating an area of 0,73 km², and infilling a topographic range from 165 up to 330 MASL. During phase 3, the lava spread towards the northeast and the southern region of the valley reaching an area of 2,07 km² and covering elevations from 164 up to 320 MASL. The lava flow path delineated for phase 4 also exhibited movement to the east and the south and infilled a topographic range from 110 to 347 MASL; besides, it presented the largest extent among the eruptive phases resulting in an area of 4,10 km². The post-eruption phase showed small changes that covered elevations from 113 up to 310 MASL in the northern and south-western regions, reaching an area of 4,32 km².

The difference in delineated area when comparing the OBIA results and the reference data is more significant for the post-eruption phase than for the syn-event phases and is less notable for the syn-eruptive phases 2 and 3 (Table 7). The negative values in the difference indicate that the OBIA delineation for the specific event resulted in less area compared to the reference data, and conversely, a positive value means that the OBIA outline resulted in more area than the reference data. Negative values were obtained for phases 2, 3 and the post-eruption, and positive values were obtained for the syn-eruptive phases 1 and 4 (Table 7). In general, the accuracy values are similar for the OBIA and the orthophotos delineation created by Pedersen et al. (2022). Figure 26 displays the accuracy assessment results in the form of a line chart and indicates how the accuracies changed through time. The producer's accuracy ranges from 82 to 96 percent, being the post-eruption the event with the highest value, and the phase 1, the event with the lowest value. On the other hand, the user's accuracy presents values varying from 86 to 92, 85 percent associated to the post-eruption event and 91 percent related to phase 3. For the overall accuracy, the lowest value is 84 percent, and the highest value is 92 percent.

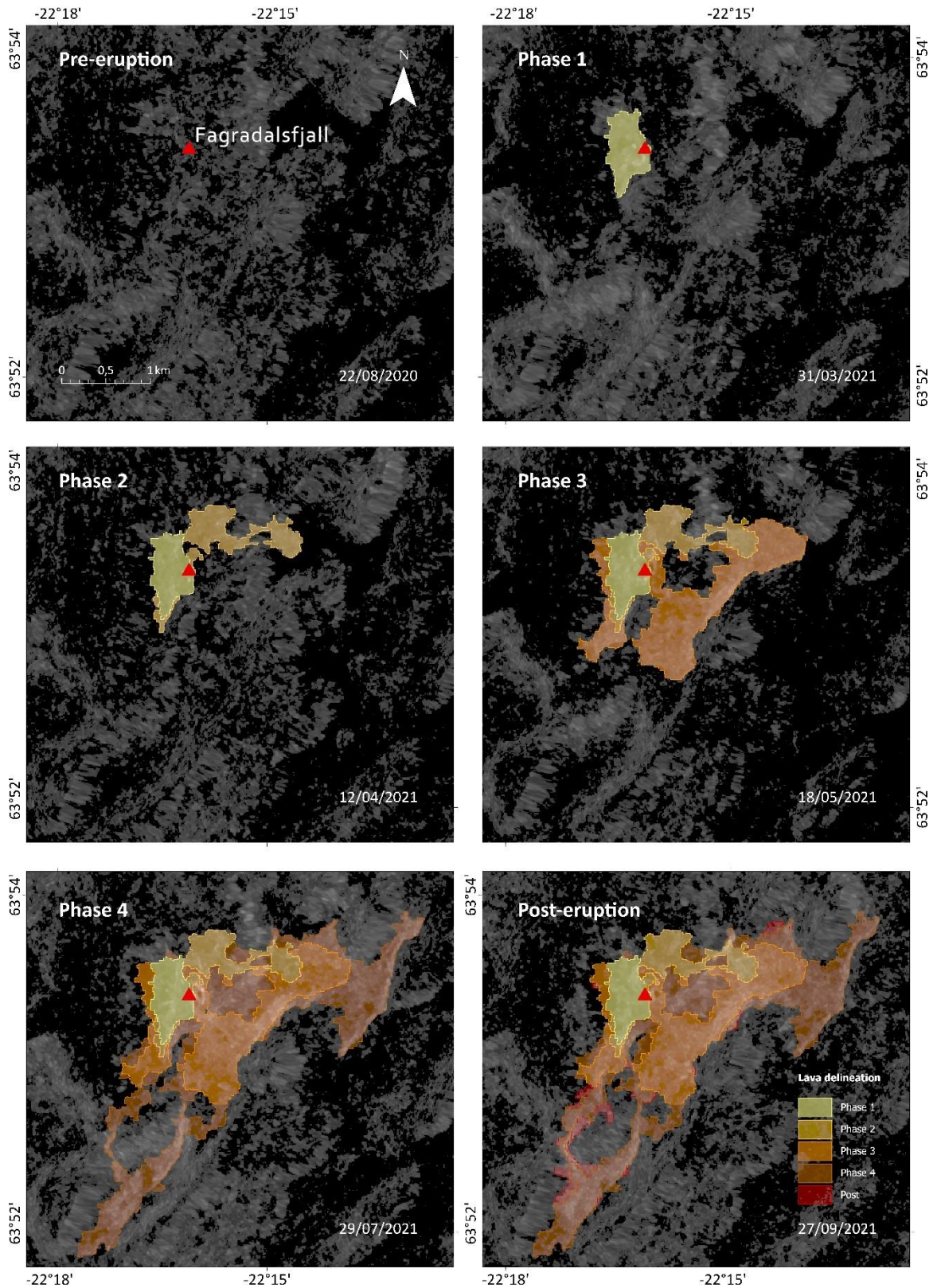


Figure 25: Resulting lava flow delineations for each eruptive phase extracted with OBIA and visualised on top of the corresponding Sentinel-1 imagery.

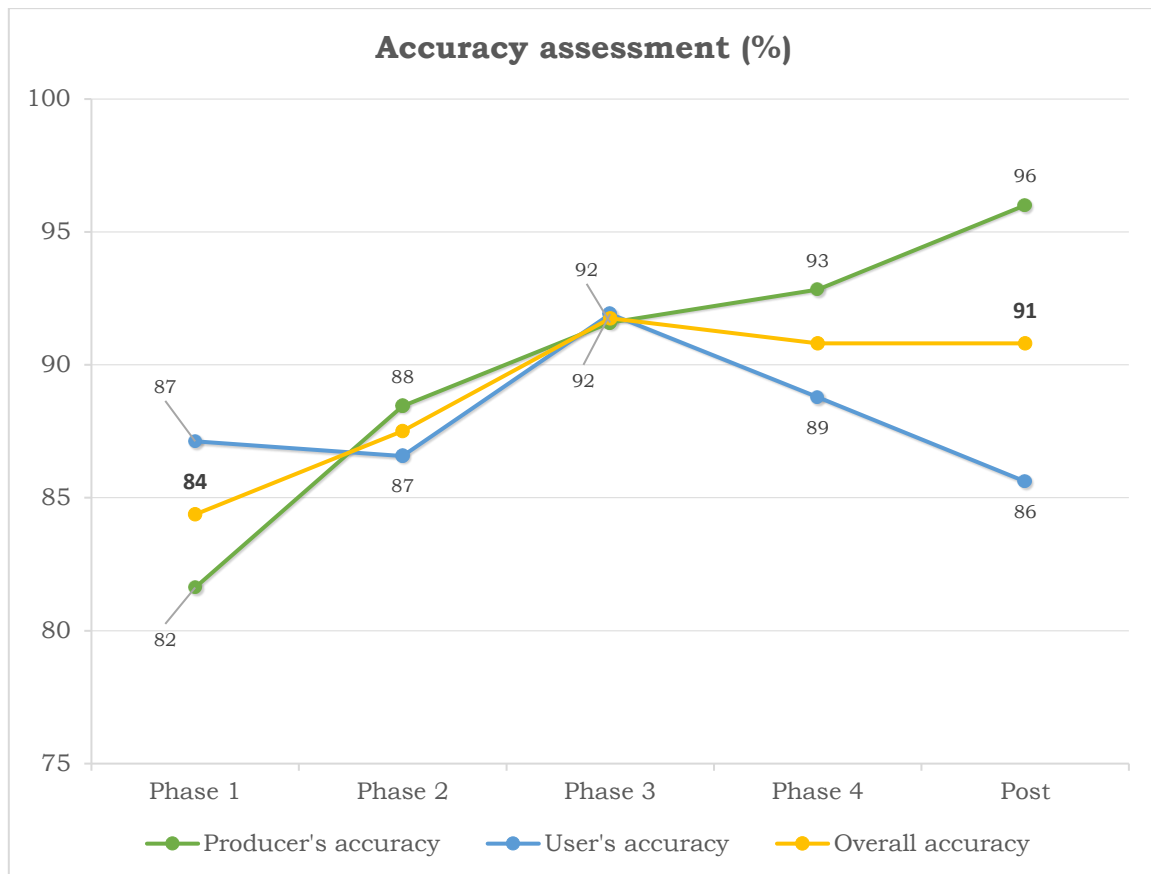


Figure 26: Results of the accuracy assessment showing the obtained producer's accuracy (OBIA extraction) and the user's accuracy (reference data).

6.2 Visualisation results

3D Web Map Application

The GitHub repository containing all the files associated with the web map application is accessible at: <https://github.com/s1085496/FagradalsfjallApp>.

Figure 27 shows an overview of the web map application which can also be found under the following link: [Fagradalsfjall Application](#). The application consists of several widgets, labels, and controls that support the interactivity of the interface. The components are enumerated as follows:

1. Header label to the top-left corner of the web application that displays the title and footer label to the lower-left corner displaying the data sources and attribution.
2. Dynamic north arrow to the lower-left corner of the web application.
3. Navigation widget that displays the orientation and position of the scene in X,Y, Z.
4. The narrative screen shows the narrative and multimedia content associated to the animation keyframes. The narrative content changes every time the animation starts or manually by clicking the next arrow button.

5. The main web map frame displaying the 3D scene which can be moved according to the following orbit controls:

Table 8: Orbit controls of the web map application. Taken and modified from qgis2threejs tutorial available at:

<https://buildmedia.readthedocs.org/media/pdf/qgis2threejs/docs/qgis2threejs.pdf>

Control	Keys	
	Mouse	Touch
Orbit	Left button	One finger move
Zoom	Scroll wheel	Two-finger spread
Pan	Right button	Two-finger move

6. The “dat-gui” panel on the top-right corner shows all the layers that are contained within the map frame including the raster and vector data. The controls are divided in three main sections:
 - a. Layers: The layers section includes the raster and vector data that displays a check box to toggle the layer visibility. And the opacity can be changed either by hovering over the slider or by modifying the number next to the slider.
 - b. Animation: Allows to pause or play the animation.
 - c. Help: Redirects the user to the help page that describes the website usage keys.

The CSS file was modified to customise the background colour of the web application and the styling of the labels and widgets.

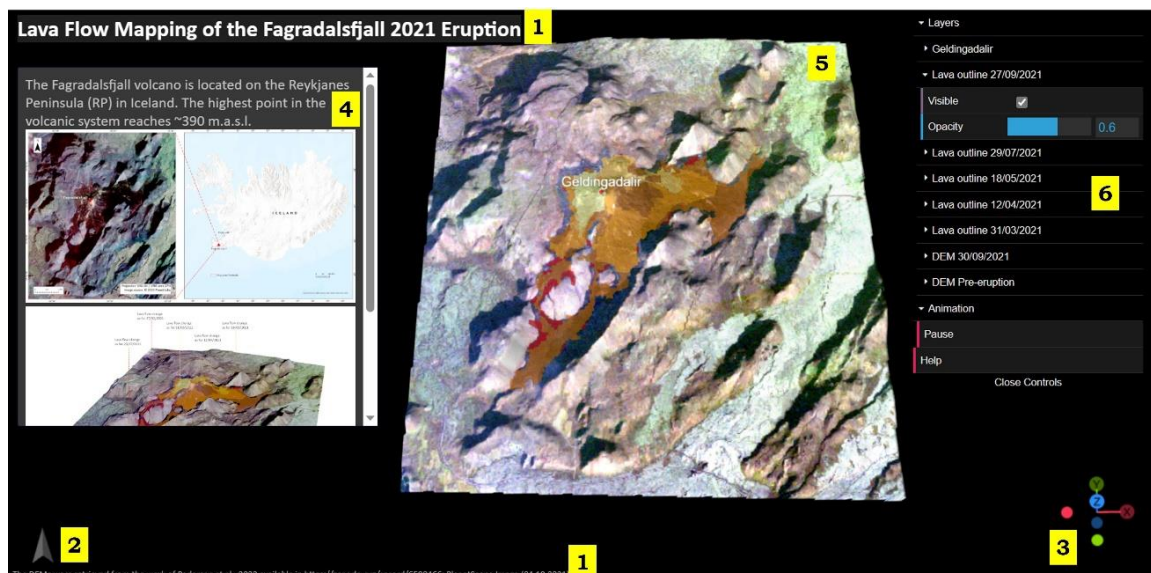


Figure 27: Overview of the 3D Web Map application hosted in GitHub and main functionalities and sections from 1 to 6.

7 DISCUSSION

Data suitability

The SAR data used for this research is open source. Open-source datasets are easily accessible and the process of retrieving the data is faster and more efficient especially when the data can be downloaded from user-friendly portals such as ASF. The main reasons considered to select SAR data to map the lava flows of the 2021 Fagradalsfjall eruption were the weather independence capabilities, the stability of the imaging conditions, and the consistent imaging modes of the SAR sensing systems. The all-day and night ability to provide imagery allows to track natural dynamic processes such as volcanic eruptions in near real-time. SAR sensors have their own illumination source which provides highly stable imaging conditions that are fundamental to thoroughly detect changes caused by the spread of lava flows. Besides, SAR is a modern sensor with consistent imaging modes that allow it to have both high-resolution and wide spatial coverage at the same time, resulting in SAR harmonized data archives and better capabilities for change detection. Sentinel-1 satellites provide global coverage, have a spatial resolution of 10 meters, and a revisiting cycle of 6 days with both of its satellites for the entire orbit. Despite the high spatial resolution of the datasets used for the extraction of the lava flows, it could represent a limiting factor compared to the small spatial extent of the study area.

The main challenges of using radar imagery for lava flow mapping were the geometric distortions, the speckle noise in the imagery, and the regular or background image content masking subtle change signatures. The geometric distortions associated with the side-looking geometry of SAR systems are foreshortening, layover, and shadow effects. Foreshortening can make the objects appear smaller because it creates a projective contraction of the image, layover can lead to ghost features, and shadow effects can hide image attributes. The regular or background information of the image can disrupt the recognition of potential changes. Additionally, the salt and pepper effect that comes intrinsically with SAR imagery can make it harder to perform change detection analysis because it can alter the appearance of lava flow shapes and structures. The terrain correction applied during the data pre-processing could have improved the geometric representation of the image, helping to reduce the effects of the distortions. Furthermore, speckle filtering was applied to the datasets used in the analysis with the aim of reducing the salt-and-pepper effect in the images.

The 30 meters resolution Copernicus DEM was used for the radiometric terrain correction and the time frame of data acquisition of this DEM ranges from 2011 to 2015. This layer was used for processing the terrain correction of all of the images, including the pre-, syn-, and post-eruption events, which means that the topographic changes at the time of each SAR image were not considered in the analysis. Neglecting the differences in topography caused that some parts of the lava flow path in the syn-eruptive phases and the post-eruption could not be extracted, especially for the areas where the topography exhibited the greatest changes. This issue could have been better addressed if the terrain correction was performed at least with pre- and post-eruption DEMs or with elevation models for which the date relatively matched with the date of each analysed image. For

instance, interferometric techniques could have been applied to the same Sentinel-1 data used for the analysis in order to generate multi-temporal DEMs.

Potential and limitations of the lava flow mapping methodology

The analysis of SAR backscatter using OBIA showed great potential to map the lava flow deposits of the 2021 Fagradalsfjall eruption. The accuracy of the mapping outlines generated with OBIA was assessed by comparing them to lava outlines delineated manually using orthophotos by Pedersen et al. (2022) (Table 7). The accuracy assessment indicated high coincidence with the reference data, obtaining overall accuracies above 80 percent for all of the analysed phases. The total lava flow path area obtained from OBIA was 4,3 km² while the reference data covers 4,8 km². The difference in area indicates underestimation of the lava flow deposits. This can be related to the limitations of the data used for the analysis, the classification scheme developed for the extraction, and the sensitivity of the approach to the image objects derived from the multiresolution segmentation. For instance, segments enclosing known areas of existing lava displayed very different backscattering intensity values, excluding them from the lava classification. The differences in the backscattering properties presented by these segments could be associated with the elevation surface used to apply the radiometric terrain flattening and the terrain correction pre-processing steps on the radar images (see discussion section on data suitability). Furthermore, the segmentation and the classification schemes were developed based on knowledge-based and trial-and-error approaches which introduce a degree of subjectivity into the classification. Thus, objects displaying very low backscattering change magnitudes, with lower internal homogeneity, or with diffuse borders were difficult to integrate within the classification scheme and this could also have led to the classification of false-positive and true-negative lava segments.

The main object-based feature used for the semi-automatic classification was an arithmetic layer that calculated the difference in backscattering between two consecutive pairs of images, representing the change from one phase to the next one (subtraction layer). The SL proved to be useful for the lava classification among all the phases because of the contrasting differences that it displayed between the lava class and the surrounding objects. Additionally, using the already classified lava segments as thematic layers every time the next segmentation was performed allowed to maintain the integrity of the time-series analysis. This was considered because when applying OBIA for time-series analysis it is very unlikely to obtain the exact same segments from image to image, even when the imaging conditions and the classification parameters are the same. The thresholds and parametrisation values used for mapping the lava flows were specifically tested for the case of the 2021 Fagradalsfjall eruption; however, further research could test the transferability of the approach and the applicability of SL values in object-based classification schemes for different volcanoes around the world.

Insights from the lava flows visualisations

The main difficulties faced during the development of the 3D web map animation were the integration of several EO datasets and the selection of a suitable platform or software that allowed interactivity and fast rendering. Overlaying the resulting lava flow outlines (2D vector data) on top of the elevation surfaces in the qgis2threejs platform required the

conversion of the vector datasets to multipatch because the projection of the layers in 3D was not automatic. Finding the best matching parameters to assign elevation values to the vector layers was time-consuming and the file format had to be changed several times to bring the layers from one GIS software to another. Several platforms were tested before `qgis2threejs` including ArcGIS Pro, City Engine, Blender, and Cesium ion. The main reasons to choose the QGIS plugin were: it is an open-source product, allows fast rendering, interactivity, and animations, and it is easy to use. Compared to ArcGIS Online and City Engine, `qgis2threejs` does not require any licensing or payment. Additionally, ArcGIS Online does not support 3D animations and the layers rendering is very slow, and City Engine is harder to manage, and depending on the data, the rendering can be very slow such as in the case of very-high-resolution DEMs. Blender required an excessive amount of time and hardware resources to create elevation surfaces from the very-high resolution pre- and post-eruption DEMs. Cesium ion allows fast rendering and is a user-friendly platform to build 3D applications; however, customisation of vector layers is not allowed for the open version, and it is not possible to interact with the layers when the application is published.

Some of the limitations found in the `qgis2threejs` plugin were that once the vector layers are added to the 3D scene, there is only one layer configuration that can be displayed in the different keyframes of the animation. This can affect the storytelling purpose of the application because the scene is not understood as a progressive story. Besides, the default styling of the webpage looks antique and because of the large archive that is generated after exporting the application, it can be hard to edit the styling in the native files. Future research could evaluate qualitatively and quantitatively how effectively the 3D visualisations are contributing to communicating the research results to the users.

8 CONCLUSION

The aim of this study was to evaluate the potential of SAR data in semi-automated lava flow mapping using OBIA and to determine the extent of the lava flow for the 2021 Fagradalsfjall eruption. The objectives were to perform a time-series analysis using Sentinel-1 data and OBIA to delineate the extent of the lava flows, to assess the accuracy of the results by comparing them to existing delineations, and to visualise the lava fields interactively by creating a 3D animated web map application.

To achieve the semi-automatic lava flows delineation, the OBIA approach was applied to SAR data. The procedure required pre-processing of the data, image segmentation and classification for extracting the lava flows, and validation of the delineated lava flow outlines. The accuracy assessment of the results showed a high correlation with the reference data and overall accuracies above 80 percent were obtained. The lava flow field covered 4,3 km², ten percent less than the area reported for the reference data. Yet the use of OBIA in semi-automated lava flow mapping is relatively new, especially when using Sentinel-1 as the basis for analysis, the outcomes exhibited promising accuracy.

A 3D interactive visualisation of the lava flows was created and openly shared through the web to communicate the research results to the general public. The web map application was hosted in GitHub under the following link: [Fagradalsfjall Application](#). The visualisation consists of several interactive widgets and controls and includes animation and multimedia support. The application provides meaningful information associated with the lava flow mapping and might improve the readability of the results for diverse groups of users.

In conclusion, this study revealed the high potential of using OBIA on Sentinel-1 backscatter data for mapping the lava flows of the 2021 Fagradalsfjall volcano and provided an interactive web application to communicate the results. Nevertheless, limitations associated with the SAR data and the sensitivity of the method to the chosen image objects' parametrisation and classification scheme should be considered to obtain high-quality results. Future research ought to further explore the potential of using OBIA and the intensity backscattering information recorded by SAR data for semi-automatic mapping of worldwide lava flows. The outcomes of the research could be used as ground data for upcoming studies in the area. Additionally, the information contained in the lava flow maps can contribute to a better understating of the lava flow model and can support local authorities to thoroughly respond against volcanic hazards.

REFERENCES AND INFORMATION SOURCES

- Aditiya, A., Aoki, Y., & Anugrah, R. D. (2018). Surface deformation monitoring of Sinabung volcano using multi temporal InSAR method and GIS analysis for affected area assessment. *IOP Conference Series: Materials Science and Engineering*, 344(1). <https://doi.org/10.1088/1757-899X/344/1/012003>
- Albino, F., Smets, B., D'Oreye, N., & Kervyn, F. (2015). High-resolution TanDEM-X DEM: An accurate method to estimate lava flow volumes at Nyamulagira Volcano (D. R. Congo). *Journal of Geophysical Research: Solid Earth*, 120(6), 4189–4207. <https://doi.org/10.1002/2015JB011988>
- Antoniou, V., Nomikou, P., Panousis, D., & Zafeirakopoulou, E. (2021). Nisyros volcanic island: A geosite through a tailored gis story. *Geosciences (Switzerland)*, 11(3). <https://doi.org/10.3390/geosciences11030132>
- Antoniou, V., Ragia, L., Nomikou, P., Bardouli, P., Lampridou, D., Ioannou, T., Kalisperakis, I., & Stentoumis, C. (2018). Creating a story map using geographic information systems to explore geomorphology and history of Methana peninsula. *ISPRS International Journal of Geo-Information*, 7(12). <https://doi.org/10.3390/ijgi7120484>
- Aufaristama, M., Hölbling, D., Höskuldsson, Á., & Jónsdóttir, I. (2017). Comparison of SAM and OBIA as Tools for Lava Morphology Classification-A Case Study in Krafla, NE Iceland. *EGU General Assembly Conference Abstracts*, 16478.
- Barsotti, S., Parks, M. M., Pfeffer, M. A., Óladóttir, B. A., Barnie, T., Titos, M. M., Jónsdóttir, K., Pedersen, G. B. M., Hjartardóttir, R., Stefansdóttir, G., Johannsson, T., Arason, Gudmundsson, M. T., Oddsson, B., Prastarson, R. H., Ófeigsson, B. G., Vogfjörð, K., Geirsson, H., Hjörvar, T., ... Sigurðsson, E. M. (2023). The eruption in Fagradalsfjall (2021, Iceland): how the operational monitoring and the volcanic hazard assessment contributed to its safe access. *Natural Hazards*. <https://doi.org/10.1007/s11069-022-05798-7>
- Blaschke, T. (2005). Towards a framework for change detection based on image objects. *Göttinger Geographische Abhandlungen*, 113, 1–9.
- Blaschke, T. (2010). Object based image analysis for remote sensing. In *ISPRS Journal of Photogrammetry and Remote Sensing* (Vol. 65, Issue 1, pp. 2–16). <https://doi.org/10.1016/j.isprsjprs.2009.06.004>
- Chen, G., Hay, G. J., Carvalho, L. M. T., & Wulder, M. A. (2012). Object-based change detection. In *International Journal of Remote Sensing* (Vol. 33, Issue 14, pp. 4434–4457). Taylor and Francis Ltd. <https://doi.org/10.1080/01431161.2011.648285>
- Cigna, F., Tapete, D., & Lu, Z. (2020). Remote sensing of volcanic processes and risk. In *Remote Sensing* (Vol. 12, Issue 16). MDPI AG. <https://doi.org/10.3390/RS12162567>

- Clifton, A. E., & Kattenhorn, S. A. (2006). Structural architecture of a highly oblique divergent plate boundary segment. *Tectonophysics*, 419(1–4), 27–40. <https://doi.org/10.1016/j.tecto.2006.03.016>
- Congalton, R. G. (1991). *A Review of Assessing the Accuracy of Classifications of Remotely Sensed Data* (Vol. 37).
- Dierking, W., & Haack, H. (1998). L-band polarimetric SAR-signatures of lava flows in the Northern Volcanic Zone, Iceland. *IGARSS '98. Sensing and Managing the Environment. 1998 IEEE International Geoscience and Remote Sensing. Symposium Proceedings. (Cat. No.98CH36174)*, 3, 1339–1341 vol.3. <https://doi.org/10.1109/IGARSS.1998.691402>
- Dirscherl, M., & Rossi, C. (2018). Geomorphometric analysis of the 2014–2015 Bárðarbunga volcanic eruption, Iceland. *Remote Sensing of Environment*, 204, 244–259. <https://doi.org/10.1016/j.rse.2017.10.027>
- Dumont, S., Sigmundsson, F., Parks, M. M., Drouin, V. J. P., Pedersen, G. B. M., Jónsdóttir, I., Höskuldsson, Á., Hooper, A., Spaans, K., Bagnardi, M., Gudmundsson, M. T., Barsotti, S., Jónsdóttir, K., Högnadóttir, T., Magnússon, E., Hjartardóttir, Á. R., Dürig, T., Rossi, C., & Oddsson, B. (2018). Integration of SAR Data Into Monitoring of the 2014–2015 Holuhraun Eruption, Iceland: Contribution of the Icelandic Volcanoes Supersite and the FutureVolc Projects. *Frontiers in Earth Science*, 6. <https://doi.org/10.3389/feart.2018.00231>
- Ebmeier, S. K., Biggs, J., Mather, T. A., Elliott, J. R., Wadge, G., & Amelung, F. (2012). Measuring large topographic change with InSAR: Lava thicknesses, extrusion rate and subsidence rate at Santiaguito volcano, Guatemala. *Earth and Planetary Science Letters*, 335–336, 216–225. <https://doi.org/10.1016/j.epsl.2012.04.027>
- Feizizadeh, B., Kazemi Garajeh, M., Blaschke, T., & Lakes, T. (2021). An object-based image analysis applied for volcanic and glacial landforms mapping in Sahand Mountain, Iran. *Catena*, 198. <https://doi.org/10.1016/j.catena.2020.105073>
- Filipponi, F. (2019). Sentinel-1 GRD Preprocessing Workflow. *Proceedings*, 18. <https://doi.org/10.3390/ecrs-3-06201>
- Global Volcanism Program. (2021). Report on Fagradalsfjall (Iceland). *Bulletin of the Global Volcanism Network*, 46(10).
- Gudmundsson, M. T., Larsen, G., Höskuldsson, Á., & Gylfason, Á. G. (2008). Volcanic hazards in Iceland. *Jökull*, 58, 251–268.
- Harris, A. J. L. (2015). Chapter 2 - Basaltic Lava Flow Hazard. In J. F. Shroder & P. Papale (Eds.), *Volcanic Hazards, Risks and Disasters* (pp. 17–46). Elsevier. <https://doi.org/https://doi.org/10.1016/B978-0-12-396453-3.00002-2>
- Hölbling, D., Aufaristama, M., & Dabiri, Z. (2019). Object-based Image Analysis for Lava Flow Morphology Classification using Optical and SAR Satellite Imagery. *27th IUGG General Assembly 2019*.

- Höskuldsson, Á., Hey, R., Kjartansson, E., & Gudmundsson, G. B. (2007). The Reykjanes Ridge between 63°10'N and Iceland. *Journal of Geodynamics*, 43(1), 73–86. <https://doi.org/10.1016/j.jog.2006.09.003>
- Kubanek, J., Richardson, J. A., Charbonnier, S. J., & Connor, L. J. (2015). Lava flow mapping and volume calculations for the 2012–2013 Tolbachik, Kamchatka, fissure eruption using bistatic TanDEM-X InSAR. *Bulletin of Volcanology*, 77(12), 1–13. <https://doi.org/10.1007/s00445-015-0989-9>
- Kyriou, A., & Nikolakopoulos, K. G. (2022). Lava Mapping Using Sentinel-1 Data after the Occurrence of a Volcanic Eruption—The Case of Cumbre Vieja Eruption on La Palma, Canary Islands, Spain. *Sensors*, 22(22). <https://doi.org/10.3390/s22228768>
- Lamb, O. D., Gestrich, J. E., Barnie, T. D., Jónsdóttir, K., Ducrocq, C., Shore, M. J., Lees, J. M., & Lee, S. J. (2022). Acoustic observations of lava fountain activity during the 2021 Fagradalsfjall eruption, Iceland. *Bulletin of Volcanology*, 84(11). <https://doi.org/10.1007/s00445-022-01602-3>
- Pedersen, G. B. M. (2016). Semi-automatic classification of glaciovolcanic landforms: An object-based mapping approach based on geomorphometry. *Journal of Volcanology and Geothermal Research*, 311, 29–40. <https://doi.org/10.1016/j.jvolgeores.2015.12.015>
- Pedersen, G. B. M., Belart, J. M. C., Óskarsson, B. V., Gudmundsson, M. T., Gies, N., Högnadóttir, T., Hjartardóttir, Á. R., Pinel, V., Berthier, E., Dürig, T., Reynolds, H. I., Hamilton, C. W., Valsson, G., Einarsson, P., Ben-Yehosua, D., Gunnarsson, A., & Oddsson, B. (2022). Volume, Effusion Rate, and Lava Transport During the 2021 Fagradalsfjall Eruption: Results From Near Real-Time Photogrammetric Monitoring. *Geophysical Research Letters*, 49(13). <https://doi.org/10.1029/2021GL097125>
- Pinel, V., Poland, M. P., & Hooper, A. (2014). Volcanology: Lessons learned from Synthetic Aperture Radar imagery. In *Journal of Volcanology and Geothermal Research* (Vol. 289, pp. 81–113). Elsevier B.V. <https://doi.org/10.1016/j.jvolgeores.2014.10.010>
- Richter, N., & Froger, J. L. (2020). The role of Interferometric synthetic aperture radar in detecting, mapping, monitoring, and modelling the volcanic activity of piton de la Fournaise, La Reunion: A review. In *Remote Sensing* (Vol. 12, Issue 6). MDPI AG. <https://doi.org/10.3390/rs12061019>
- Robb, C., Willis, I., Arnold, N., & Gudmundsson, S. (2015). A semi-automated method for mapping glacial geomorphology tested at Breidamerkurjökull, Iceland. *Remote Sensing of Environment*, 163, 80–90. <https://doi.org/10.1016/j.rse.2015.03.007>
- Romero, R., Fernández, J., Carrasco, D., Luzón, F., Martínez, A., Rodríguez-Velasco, G., Moreno, V., Araña, V., & Aparicio, A. (2002). *Física de la Tierra Synthetic Aperture Radar Interferometry (InSAR): Application to ground deformation studies for volcano and seismic monitoring*. 14, 55–84.

- Rösch, M., & Plank, S. (2022). Detailed Mapping of Lava and Ash Deposits at Indonesian Volcanoes by Means of VHR PlanetScope Change Detection. *Remote Sensing*, 14(5). <https://doi.org/10.3390/rs14051168>
- Rosen, P. A., Hensley, S., Joughin, I. R., Li, F. K., Madsen, S. N., Rodríguez, E., & Goldstein, R. M. (2000). Synthetic Aperture Radar Interferometry. *Proceedings of the IEEE*, 88(3), 333–382.
- Roth, R. E. (2021). Cartographic Design as Visual Storytelling: Synthesis and Review of Map-Based Narratives, Genres, and Tropes. *Cartographic Journal*, 58(1), 83–114. <https://doi.org/10.1080/00087041.2019.1633103>
- Sæmundsson, K., Sigurgeirsson, M., & Friðleifsson, G. Ó. (2020). Geology and structure of the Reykjanes volcanic system, Iceland. *Journal of Volcanology and Geothermal Research*, 391. <https://doi.org/10.1016/j.jvolgeores.2018.11.022>
- Samsonov, S., & d'Oreye, N. (2012). Multidimensional time-series analysis of ground deformation from multiple InSAR data sets applied to Virunga Volcanic Province. *Geophysical Journal International*, 191(3), 1095–1108. <https://doi.org/10.1111/j.1365-246X.2012.05669.x>
- Sigmundsson, F., Parks, M., Hooper, A., Geirsson, H., Vogfjörð, K. S., Drouin, V., Ófeigsson, B. G., Hreinsdóttir, S., Hjaltadóttir, S., Jónsdóttir, K., Einarsson, P., Barsotti, S., Horálek, J., & Ágústsdóttir, T. (2022). Deformation and seismicity decline before the 2021 Fagradalsfjall eruption. *Nature*, 609(7927), 523–528. <https://doi.org/10.1038/s41586-022-05083-4>
- Smets, B., Wauthier, C., & d'Oreye, N. (2010). A new map of the lava flow field of Nyamulagira (D.R. Congo) from satellite imagery. *Journal of African Earth Sciences*, 58(5), 778–786. <https://doi.org/10.1016/j.jafrearsci.2010.07.005>
- Thöny, M., Schnürer, R., Sieber, R., Hurni, L., & Pajarola, R. (2018). Storytelling in interactive 3D geographic visualization systems. *ISPRS International Journal of Geo-Information*, 7(3). <https://doi.org/10.3390/ijgi7030123>
- Trimble Germany GmbH. (2022). Trimble Documentation eCognition Developer 10.3 Reference Book. *Trimble Germany GmbH*.
- Veenendaal, B., Brovelli, M. A., & Li, S. (2017). Review of web mapping: Eras, trends, and directions. In *ISPRS International Journal of Geo-Information* (Vol. 6, Issue 10). MDPI AG. <https://doi.org/10.3390/ijgi6100317>
- Zhou, X., Chang, N. Bin, & Li, S. (2009). Applications of SAR interferometry in earth and environmental science research. In *Sensors* (Vol. 9, Issue 3, pp. 1876–1912). <https://doi.org/10.3390/s90301876>

ATTACHMENTS

LIST OF ATTACHMENTS

Free attachments

Attachment 1 Poster

Attachment 2 Website